

**University of Plymouth**

**PEARL**

**<https://pearl.plymouth.ac.uk>**

---

Faculty of Science and Engineering

School of Geography, Earth and Environmental Sciences

---

2019-06

# Sea ice control on winter subsurface temperatures of the North Iceland Shelf during the Little Ice Age: A TEX<sub>86</sub> calibration case study

David J. Harning<sup>1, 2, 3 \*</sup>, John T. Andrews<sup>2</sup>, Simon T. Belt<sup>4</sup>, Patricia Cabedo-Sanz<sup>4</sup>, Nadia Dildar<sup>2, 3</sup>, Áslaug Geirsdóttir<sup>1</sup>, Gifford H. Miller<sup>1, 2</sup>, Julio Sepúlveda<sup>2, 3 \*</sup>

<sup>1</sup> Faculty of Earth Sciences, University of Iceland, Reykjavík, Iceland

<sup>2</sup> INSTAAR and Department of Geological Sciences, University of Colorado Boulder, Boulder, CO, USA

<sup>3</sup> Organic Geochemistry Laboratory, University of Colorado Boulder, Boulder, CO, USA

<sup>4</sup> Biogeochemistry Research Centre, School of Geography, Earth and Environmental Sciences, Plymouth University, Plymouth, UK

\* Corresponding authors

David J. Harning and Julio Sepúlveda

Email: [david.harning@colorado.edu](mailto:david.harning@colorado.edu); [jsepulveda@colorado.edu](mailto:jsepulveda@colorado.edu)

**Journal:** *Paleoceanography and Paleoclimatology*

## Key Points:

- 1) Our local Icelandic GDGT calibration produces more realistic temperature estimates with substantially lower uncertainty over broader spatial calibrations
- 2) Periods of thick sea ice during the Little Ice Age likely warmed the subsurface as a result of winter insulation

**Keywords:** North Iceland Shelf, marine sediment, Little Ice Age, lipid biomarkers, IP<sub>25</sub>, GDGTs

## Abstract

Holocene paleoceanographic reconstructions along the North Iceland Shelf (NIS) have employed a variety of sea-surface temperature (SST) and sea-ice proxies. However, these surface proxies tend to have a seasonal bias toward spring/summer, and thus, only provide a discrete snapshot of surface conditions during one season. Furthermore, SST proxies can be influenced by additional confounding variables resulting in markedly different Holocene temperature reconstructions. Here, we expand Iceland’s marine paleoclimate toolkit with TEX<sub>86</sub><sup>L</sup>; a temperature proxy based on the distribution of archaeal glycerol dibiphytanyl glycerol tetraether (GDGT) lipids. We develop a local Icelandic calibration from 21 surface sediment samples covering a wide environmental gradient across Iceland’s insular shelves. Locally calibrated GDGT results demonstrate that: 1) TEX<sub>86</sub><sup>L</sup> reflects winter subsurface (0-200 m) temperatures on the NIS, and 2) our calibration produces more realistic temperature estimates with substantially lower uncertainty (S.E.  $\pm 4$  °C) over global calibrations. We then apply this new calibration to a high-resolution marine sediment core (last millennium) collected from the central NIS (B997-316 GGC, 658 m depth) with age control constrained by <sup>14</sup>C-dated mollusks. To test the veracity of the GDGT subsurface temperatures, we analyze quartz and calcite wt% and a series of highly branched isoprenoid alkenes, including the sea ice biomarker IP<sub>25</sub>, from the same core. The sediment records demonstrate that the development of thick sea ice during the Little Ice Age warmed the subsurface due to winter insulation. Importantly, this observation reflects a seasonal component of the sea-ice/ocean feedback to be considered for the non-linear cooling of the Little Ice Age in and around Iceland.

## 1. Introduction

The steep oceanographic (temperature, salinity, and nutrient) gradients caused by the presence of Arctic and Atlantic Ocean currents surrounding Iceland have made the insular shelves targets for northern North Atlantic climate change studies since the last deglaciation (Knudsen et al., 2004; Ólafsdóttir et al., 2010). Throughout the Holocene, the strength and latitudinal position of these currents has varied on centennial timescales, impacting terrestrial climate (Larsen et al., 2012; Geirsdóttir et al., 2013, 2019; Harning et al., 2018), as well as the status of Icelandic ice caps (Larsen et al., 2011; Brynjólfsson et al., 2015; Harning et al., 2016a, 2016b; Anderson et al., 2018). As the North Atlantic is the region that exhibits the largest meridional heat flux of the Northern Hemisphere (Wunsch, 1980), and the area of deep-water formation that drives the Atlantic Meridional Overturning Circulation (AMOC), changes in local climate also have widespread hemispheric relevance (Denton & Broecker, 2008; Buckley & Marshall, 2016). Thus, gaining a more comprehensive understanding of the past oceanographic conditions in this region of the North Atlantic is not only key to understanding past episodes of climate change, but also critical to contextualize circulation changes under a currently warming climate (Spielhagen et al., 2011; Caesar et al., 2018; Thornalley et al., 2018).

Over recent decades, numerous marine sediment core studies have generated surface and bottom water temperature proxy records based on Mg/Ca and  $\delta^{18}\text{O}$  of benthic and planktic foraminifera, calcite wt%, the alkenone unsaturation index ( $U_{37}^k$ ) and biotic species assemblages, such as dinoflagellates and diatoms (Andersen et al., 2004; Castañeda et al., 2004; Giraudeau et al., 2004; Smith et al., 2005; Solignac et al., 2006; Bendle & Rosell-Melé, 2007; Justwan et al., 2008; Ran et al., 2008; Ólafsdóttir et al., 2010; Jiang et al., 2015; Moossen et al., 2015; Kristjánsdóttir et al., 2016). Sea surface temperature (SST)

proxies derived from phytoplankton result in a bias toward spring/summer SST and are influenced by additional confounding variables (i.e., salinity, nutrients, and depth habitat of biota, e.g., [Prahl et al., 2006](#); [Chival et al., 2014](#)), resulting in markedly different Holocene temperature reconstructions around Iceland ([Kristjánsdóttir et al., 2016](#)). As an example, the Little Ice Age (LIA, 1250-1850 CE) is believed to be the coldest multi-centennial climate anomaly of the Holocene in Iceland, yet the coldest Holocene conditions inferred from alkenones ([Kristjánsdóttir et al., 2016](#)), dinocysts ([Solignac et al., 2006](#)) and diatoms ([Andersen et al., 2004](#); [Justwan et al., 2008](#)) occur earlier, between 4 and 2 ka. Although the cooling observed in some proxies between 4 and 2 ka may be linked to long-term changes in the AMOC ([Hall et al., 2004](#)) and/or North Atlantic Oscillation ([Orme et al., 2018](#)), expanding Iceland’s quantitative proxy toolkit may help reconcile proxy discrepancies.

In this study, we focus on quantifying the distribution of archaeal glycerol dibiphytanyl glycerol tetraethers (GDGTs) archived in marine sediment from the North Iceland Shelf (NIS). Although yet to be used to reconstruct marine paleoclimate on the NIS, GDGT distributions have been shown to reflect modern winter subsurface temperature (subT, 0-200 m) around Iceland ([Rodrigo-Gámiz et al., 2015](#)), the North Sea ([Herfort et al., 2006](#)), Skagerrak ([Rueda et al., 2009](#)), and Antarctica ([Kim et al., 2010, 2012](#)). Assuming temperature is the dominant control on the distribution of GDGTs on the NIS ([Schouten et al., 2013 and references therein](#)), but acknowledging that at least part of the variability could also be explained by confounding effects such as ammonia oxidation rates ([Hurley et al., 2016](#)), we improve absolute temperature estimates by developing a local Icelandic calibration based on the analysis of surface sediments. We then apply this

local calibration to our late Holocene marine sediment core record. A suite of additional oceanographic surface climate proxies from the same core allow us to test the veracity of and to explore controls on GDGTs-based temperatures around Iceland.

## 2. Regional Setting

Today, the NIS represents the boundary where Arctic and Atlantic Ocean currents intercept (Fig. 1a-b, [Stefánsson, 1962](#); [Hopkins, 1991](#); [Belkin et al., 2009](#)). This front separates the cool, low salinity and sea-ice-bearing East Icelandic Current (EIC, 1 to 4 °C) to the north from the warmer and more saline Atlantic waters carried by the North Iceland Irminger Current (NIIC, 5 to 8 °C) on the inner and mid-shelf ([Orvik et al., 2001](#)). The current density differences between the two water masses result in vertical stratification along the NIS, such that the NIIC overlies the denser and cooler Upper Arctic Intermediate Waters (<0 °C, UAIW) (Fig. 1c). Within 70-100 km from Iceland’s northern coastline, freshwater run-off and summer heating modify the NIIC surface waters and form “coastal surface waters” (Fig. 1c), which then disintegrate during the following winter ([Stefánsson, 1962](#); [Ólafsson et al., 2008](#)). The onset of this stratification in early spring triggers the spring bloom of phytoplankton ([Zhai et al., 2012](#)).

Atlantic waters provide the primary source of nutrients (i.e., phosphate, nitrate, silica) to the Icelandic shelves. Due to the greater influence of nutrient-deficient polar waters, NIS nutrient concentrations are considerably lower compared to those along the south of Iceland, where Atlantic waters dominate ([Stefánsson, 1968](#); [Stefánsson & Ólafsson, 1991](#)). Although the freshwater run-off from Iceland is key for the seasonal stratification and phytoplankton blooms along the NIS, it has negligible direct effects on

nitrate and phosphate concentrations throughout the water column (Stefánsson & Ólafsson, 1991). In terms of modern oxygen saturation, the eastern NIS has similar values to those of waters south of Iceland, which may suggest relatively high rates of productivity for both locations (Stefánsson & Ólafsson, 1991). However, given that the NIS is rather limited in available nutrients, the relatively high oxygen saturation on the NIS may also relate to higher solubility of the colder Arctic waters.

Sea ice is also an integral component of the NIS. Iron oxide data on detrital grains suggest that drift ice is predominately sourced from east and southeast Greenland but also from as far as Canada and Russia, with the latter distal sources dramatically increasing in abundance over the last 1 ka (Andrews et al., 2009a; Darby et al., 2017). The presence of and correlation between quartz and the IP<sub>25</sub> biomarker – proxies for sea ice extent - in core-top sediment along the NIS, and their absence from Iceland’s southern and western shelves further supports the dominance of drift ice origins over local sea ice production (Axford et al., 2011; Cabedo-Sanz et al., 2016a). When present, sea ice limits the exchange of heat, gases and moisture between the ocean and atmosphere, in addition to insulating the colder polar atmosphere from the relatively warmer ocean during winter (Thorndike et al., 1975; Maykut, 1978, 1982). Due to Iceland’s close proximity to the historical (post-1870 CE) sea ice edge (Divine & Dick, 2007), past changes in sea ice advection along the EIC have resulted in profound changes in local marine and terrestrial climate (Ogilvie & Jónsson, 2001; Moros et al., 2006; Massé et al., 2008; Miller et al., 2012; Cabedo-Sanz et al., 2016a).

### 3. Methods

#### 3.1. Surface and marine core sediments

During July 1997, the cooperative USA/Icelandic *Bjarni Sæmundsson* B997 research cruise visited 30 locations across Iceland’s western and northern shelves (Helgadóttir, 1997). At each location, marine surface sediments were collected using a grab sampler. Previous studies have used these surface samples to describe the regional distributions of foraminifera  $\delta^{18}\text{O}$  (Smith et al., 2005), quartz wt % (Andrews & Eberl, 2007), and the sea ice biomarker IP<sub>25</sub> (Axford et al., 2011; Cabedo-Sanz et al., 2016a). We selected a subset (n=11) of these marine surface sediment samples for GDGT analyses to help construct a local Icelandic calibration (Fig. 1). As many of the 30 surface sediment locations were spatially clustered, our selection provides a representative sample from each geographical location the cruise covered, and, thus optimizes our local calibration by spanning the full range of oceanographic conditions present around Iceland today. The B997 cruise also recovered a suite of piston and gravity sediment cores. In this study, we focus on giant gravity core B997-316 GGC (2.47 m long) from the central North Iceland Shelf (66.75°N, 18.79°W, 658 mbsl, Fig. 1) (Helgadóttir, 1997). Sediment (~1 cm<sup>3</sup>) was subsampled every six cm for mineralogical and biomarker analyses. In order to minimize the degradation of biomarkers (e.g., Cabedo-Sanz et al., 2016b), samples were taken from cores stored at 4 °C. All samples were subsequently freeze-dried and kept in the freezer (-20 °C) prior to biomarker extraction.

### 3.2. Age control

Four radiocarbon-based age control points are derived from a combination of mollusks (*T. equalis*) and benthic foraminifera (*N. labradorica* and *G. auriculata arctica*) sampled from the B997-316 GGC core (Table 1). As the B997-316 GGC core lacked datable material in



the uppermost sediment, two additional mollusks (*T. equalis*) were sampled from the near surface sediment of an adjacent short gravity core, B997-316 SGC (Table 1), to confirm that the tops of the sediment cores are modern and that no surface sediment was lost during coring. Samples were prepared for AMS radiocarbon dating at the Institute of Arctic and Alpine Research (INSTAAR) <sup>14</sup>C Preparation Lab and analyzed at the University of California Irvine.

### 3.3. Minerological analyses

Quantitative X-ray diffraction (qXRD) analysis was conducted on the <2 mm sediment fraction using the method developed by Eberl (2003) and used extensively on sediment samples on other B997- cores (Andrews & Eberl, 2007; Andrews et al., 2009a; Andrews, 2009). Comparison between qXRD weight percent estimates on known mineral mixtures and replicate analyses indicate that the errors on the weight percent estimates of both are in the range of  $\pm 1$  %. For B997-316 GGC, we focus on the identification of quartz as a proxy to reconstruct the incursion of drift ice into Icelandic waters (i.e., sea ice and/or icebergs), and calcite as a proxy of ocean productivity (Andrews et al., 2001).

### 3.4. Biomarker analyses

At the University of Plymouth, freeze-dried subsamples (~1-2 g) from core B997-316 GGC were extracted for biomarkers by ultrasonication using dichloromethane:methanol (2:1, v/v). Samples were initially spiked with an internal standard (9-octylheptadec-8-ene, 9-OHD, 10  $\mu$ L; 10  $\mu$ g mL<sup>-1</sup>) to permit quantification of highly branched isoprenoid (HBI) alkenes. Total lipid extracts (TLEs) were separated into three fractions (F1-F3) using silica

column chromatography, after elution with hexane (6 mL), hexane:methylacetate (80:20, v/v, 6 mL), and methanol (4 mL), respectively. The F1 fraction contained aliphatic hydrocarbons including highly branched isoprenoids (HBIs; i.e., IP<sub>25</sub>, C<sub>25:2</sub> and C<sub>25:3</sub>), whereas F2 contained lipids with hydroxyl functional groups, including GDGTs. At the University of Colorado Boulder, freeze dried marine surface sediment samples (~3-7 g) were extracted three times on a Dionex accelerated solvent extractor (ASE 200) using dichloromethane:methanol (9:1, v/v) at 100 °C and 2000 psi, and kept as TLEs for the GDGT analysis.

The IP<sub>25</sub> (C<sub>25:1</sub>), diene II (C<sub>25:2</sub>) and triene Z (C<sub>25:3</sub>) biomarkers were analyzed at the University of Plymouth as described by Belt et al. (2012, 2015). Analysis of the F1 was performed via gas chromatography-mass spectrometry (GC-MS) following the methods and operating conditions of Belt et al. (2012) on an Agilent 7890A GC coupled to a 5975 series mass selective detector fitted with an Agilent HP-5ms column (30 m x 0.25 mm x 0.25 mm). Mass spectrometric analyses were carried out in selected ion monitoring mode. The identification of IP<sub>25</sub> (Belt et al., 2007), diene II (Belt et al., 2007) and triene Z (Belt et al., 2000) was based on their characteristic GC retention indices (RI<sub>HP5MS</sub> = 2081, 2082, and 2044 for IP<sub>25</sub>, diene II, and triene Z, respectively) and mass spectra (Belt, 2018). Quantification of lipids was achieved by comparison of mass spectral responses of selected ions (IP<sub>25</sub>, *m/z* 350; diene II, *m/z* 348; triene Z, *m/z* 346) with those of the internal standard (9-OHD, *m/z* 350) and normalized according to their respective response factors and sediment masses (Belt et al., 2012). Analytical reproducibility was monitored using a standard sediment with known abundances of biomarkers for every 14-16 sediment samples extracted (analytical error 4%, n = 31).

For GDGTs, we analyzed aliquots of the F2 from B997-316 GGC and aliquots of the TLE from marine surface sediment samples in the Organic Geochemistry Laboratory at the University of Colorado Boulder. Dry samples were dissolved in hexane:isopropanol (99:1, v/v), sonicated, vortexed, and then filtered using a 0.45 µm PTFE syringe filter. Prior to analysis samples were spiked with 10 ng of the C<sub>46</sub> GDGT internal standard (Huguet et al., 2006). Isoprenoid GDGTs were identified and quantified via high performance liquid chromatography – mass spectrometry (HPLC-MS) following modified methods of Hopmans et al. (2016) on a Thermo Scientific Ultimate 3000 HPLC interfaced to a Q Exactive Focus Orbitrap-Quadrupole MS. Rather than starting at 18% hexane:isopropanol (9:1, v/v) (Hopmans et al., 2016), we began our eluent gradient with 30% hexane:isopropanol (9:1, v/v) to shorten retention and overall run times without compromising the chromatographic separation of GDGTs. The HPLC was conditioned for 20 minutes between runs. Samples were analyzed on full scan mode with a mass range of 500-1500 *m/z* at 70,000 mass resolution. GDGTs were identified based on their characteristic masses and elution patterns. We adopt the TEX<sub>86</sub><sup>L</sup> index to reflect relative changes in temperature, which is a modification of the original TEX<sub>86</sub> index (Schouten et al., 2002) constructed for temperatures <15 °C (Kim et al., 2010, 2012):

$$TEX_{86}^L = \log\left(\frac{[GDGT - 2]}{[GDGT - 1] + [GDGT - 2] + [GDGT - 3]}\right)$$

### 3.5. Local Icelandic TEX<sub>86</sub><sup>L</sup> calibration

The largest uncertainty in the temperature relationship of GDGTs in global calibrations is at the low end of the temperature spectrum (<5 °C, Kim et al., 2010, 2012), which may reflect a reduced sensitivity of Thaumarchaeota to temperature in cooler climates (Wuchter

et al., 2004) or different regional oceanographic effects. Although a recent spatially-varying, Bayesian TEX<sub>86</sub>-temperature calibration model was developed to capture regional oceanography variability (Tierney & Tingley, 2014), it excludes high-latitude settings and does not include any core top samples within a ~1000-km radius of Iceland. Hence, we targeted a network of local marine surface sediments (Fig. 1) to develop a local calibration that innately reflects the nuances of Icelandic oceanography and low local temperatures. We supplemented our 11 surface sediment samples with 10 previously published surface sediment samples from around Iceland (Table 2, Rodrigo-Gámiz et al., 2015) to generate a more comprehensive GDGT calibration that spans a larger geographical area and temperature gradient than obtainable using B997 samples alone. We note that although Rodrigo-Gámiz et al. (2015) sampled the surface of sediment cores, our samples were collected using a grab sampler, which may disturb the original sedimentary structure. However, natural factors such as sea floor mixing and variable sedimentation rates will always introduce uncertainty in the temperature embedded no matter how the sample is collected. Thus, we contend that the datasets can be merged for calibration purposes.

To calibrate the TEX<sub>86</sub><sup>L</sup> index, *in situ* decadal mean temperatures from 1995-2004 CE were obtained from the World Ocean Atlas (WOA09, Locarnini et al., 2010) at the quarter-degree pixel where each surface sediment site is located. Subsequently, seasonal (spring, summer, fall, winter) and annual SST, in addition to 0-10 m, 0-20 m, 0-30 m, 0-40 m, 0-50 m, 0-60 m, 0-70 m, 0-80 m, 0-90 m, 0-100 m, 0-125 m, 0-150 m, 0-175 m, 0-200 m depth subsurface temperature integrations, were each regressed against the 21 core top TEX<sub>86</sub><sup>L</sup> index values (Rodrigo-Gámiz et al., 2015; this study) to assess which portion

of the water column and which season the GDGT distributions most closely correspond to around Iceland. We calculated  $p$ -values for each regression to determine their significance.

## 4. Results and Interpretations

### 4.1. Age model

An age model for the B997-316 GGC sediment core was generated in the CLAM software using the Marine13 calibration curve ( $\Delta R=0$ , [Reimer et al., 2013](#)) and a smooth spline regression over 1000 iterations ([Blaauw, 2010](#)). The calibrated benthic foraminifera date from 49.5 cm depth produced an age reversal in the initial model, and thus, was identified as an outlier and removed from the final age model (Fig. 2). The ~400-year difference between the calibrated age of the foraminifera and that estimated from the model may relate to changes in  $\Delta R$  resulting from variable water masses ([Eiríksson et al., 2004](#); [Wanamaker et al., 2012](#)). The two mollusks from the adjacent short gravity core (B997-316 SGC) both returned conventional  $^{14}\text{C}$  ages  $\leq 400$  years (Table 1), confirming modern sediment at the core top of the SGC.

Based on several lines of reasoning, we argue that the modern ages of the SGC can be used to validate the extrapolation of the B997-316 GGC age model to the surface (Fig. 2). First, given that both cores were collected from the same location, we can exclude any impacts from geographic-dependent factors, such as variable sedimentation rates or oceanographic currents, that may cause the age-depth relationships to differ between the two cores. Second, coring-dependent factors can also be excluded as the two cores were collected in succession of each other using the same equipment ([Helgadóttir, 1997](#)). Even though coring operations can result in the loss of saturated or poorly consolidated surface

sediment, the identical coring techniques employed suggests that if the SGC captures modern surface sediment, so should the GGC.

Given that our age model only uses the three lowermost mollusks from the GGC and the uppermost mollusk samples from the adjacent SGC, increased age uncertainty undoubtedly exists where no datable material could be obtained (i.e., ~1400-2000 CE). However, we argue that our age estimates throughout the entire GGC core are reasonably strong. First, NIS sedimentation rate slopes only change significantly between deglacial/nonglacial periods (Andrews et al., 2002; Xiao et al., 2017) due to the presence/absence of the Icelandic Ice Sheet. Following the rapid demise of the Icelandic Ice Sheet ~15 thousand years ago (Norðdahl and Ingólfsson, 2015; Patton et al., 2017), sedimentation rates have remained linear across the NIS (Castañeda et al., 2004), consistent with the linearity of B997-316 GGC’s sedimentation rate over the last millennium (Fig. 2). Second, when our age model is applied to the proxy datasets (Fig. 3), the interpreted period of the Little Ice Age (LIA, see following section) is consistent with previous age ranges in Iceland that are derived from high-resolution and precisely-dated terrestrial archives (Geirsdóttir et al., 2009; Larsen et al., 2011, 2012).

## 4.2. Sediment core B997-316 GGC

### 4.2.1. Minerological analyses

In Icelandic waters, the two minerals quartz and calcite are qualitative indicators that reflect the incursion of drift ice (i.e., sea ice and/or icebergs) and marine surface productivity, respectively (Andrews et al., 2001, 2009a). In years when cold low-salinity Arctic water dominates, sea ice (% quartz) increases and surface productivity (% calcite) decreases due to the development of a well stratified water column. The opposite is seen in the proxies

during years characterized by warm and saline Atlantic waters, which reduces sea ice presence and mixes the water column resulting in higher productivity. Not surprisingly, % quartz and calcite generally show an inverse relationship over the last millennium in B997-316 GGC, which can be interpreted as the relative dominance of Arctic versus Atlantic waters at this location (Fig. 3a-b).

Percent quartz ranges from 1.4 to 2.7 %, whereas calcite ranges from 5.4 to 8.3 % (Fig. 3a-b). Recent analyses using mineral mixtures with known quartz wt % of 3.5 and 1.5 (Andrews et al., 2018) confirm that these small amounts of quartz can be correctly measured. Prior to ~1250 CE, quartz is relatively low, and calcite is the highest of the record, suggesting a dominance of warmer Atlantic waters at this time. Subsequently, quartz begins a gradual yet quasi-episodic rise towards its peak abundance at ~1900 CE. On the other hand, calcite appears to decline more sharply to lower values after ~1250 CE and remain relatively low through ~1900 CE, when it rises to levels near its pre-1250 CE state. Based on these two minerals, the period between 1250 and 1900 CE was likely characterized by cooler Arctic waters that favored the advection of drift ice, vertical stratification and lower surface productivity on the NIS. Following 1900 CE, the conditions reverted back to a dominance of warmer Atlantic waters that favored restricted sea drift transport and higher surface productivity (Fig. 3).

#### 4.2.2. Highly-branched isoprenoid (HBI) alkenes

The analysis of the biomarker IP<sub>25</sub> (Belt et al., 2007), a monounsaturated C<sub>25</sub> HBI biosynthesized by Arctic sea ice diatoms (Belt et al., 2008; Brown et al., 2014), has gained recent traction as a novel proxy for spring/summer sea ice conditions around Iceland (Massé et al., 2008; Andrews et al., 2009b; Sicre et al., 2013; Cabedo-Sanz et al., 2016a;

Xiao et al., 2017). Although the IP<sub>25</sub> biomarker is well-preserved in Arctic and sub-Arctic marine sediment and routinely applied in paleo sea ice reconstructions as old as 5.3 Ma (Stein et al., 2016), questions remain regarding its vertical transport, degradation processes, and environmental controls (see reviews by Belt & Müller, 2013; Belt, 2018). Notably, the interpretation of its presence (or lack thereof) can be ambiguous. IP<sub>25</sub> below the limit of detection has often been interpreted as reflecting either a lack of seasonal sea ice cover, or permanent and thick sea ice that inhibits light penetration needed for sea ice diatoms to photosynthesize and grow. However, this is likely an over-simplification of a broader range of scenarios that result in absent IP<sub>25</sub> (Belt, 2018). In any case, further information may be obtained by the complementary analysis of certain open-water phytoplankton biomarkers (i.e., brassicasterol or dinosterol, Müller et al., 2011).

Based on a distinctively heavy stable carbon isotopic composition, in addition to similar concentration profiles to IP<sub>25</sub> across Arctic marine surface sediment, the di-unsaturated HBI diene II also has an Arctic sea ice diatom source (Belt et al., 2008; Cabedo-Sanz et al., 2013; Brown et al., 2014), and is made by some Antarctic sea ice algae as well (Belt et al., 2016). In contrast, a tri-unsaturated HBI (hereafter, triene Z) is biosynthesized by certain open-water diatoms (Belt et al., 2000, 2008, 2015; Rowland et al., 2001), and sources for the Arctic and Antarctic have recently been identified (Belt et al., 2017). Importantly, the presence (or lack thereof) of triene Z, like certain phytoplankton sterols, may help differentiate between open-water or thick sea ice conditions inferred from IP<sub>25</sub> and diene II in the Arctic (Cabedo-Sanz et al., 2013; Smik et al., 2016; Köseoğlu et al., 2018). However, since sterols may also be derived from other (e.g., terrestrial) sources in



addition to sea ice algae (Huang & Meinschein, 1976; Volkman, 1986; Volkman et al., 1998; Belt et al., 2013, 2018), we limit our analysis here to triene Z only.

HBIs were detected in all downcore samples, with the exception of 96.5 cm depth (1509 CE), where no triene Z, diene II or IP<sub>25</sub> were detected (Fig. 3c-e). Concentrations ranged from near detection up to 1.6 ng/g sediment for triene Z, up to 19 ng/g sediment for diene II, and up to 4 ng/g sediment for IP<sub>25</sub>. Triene Z exhibited the highest concentrations prior to 1200 CE, while its abundance diminished to very low or undetectable between ~1200 and 1800 CE (Fig. 3c). Triene Z then rises to higher concentrations up through 2000 CE. The similar relative trends of diene II and IP<sub>25</sub> concentrations suggest that both HBIs are likely sourced from sea ice algae around Iceland, similar to other Arctic (Brown et al., 2014) and Antarctic locations (Collins et al., 2013). Periods of synchronous reductions of diene II and IP<sub>25</sub> concentrations occur at ~1170-1290 CE, 1450-1650 CE, and 1880 CE-present.

The similar overall trends between % calcite and triene Z abundance suggest that both proxies indicate temperate water surface productivity (Fig. 3b-c). Hence, in years where warmer Atlantic waters dominate, both % calcite and triene Z abundance increase, while the opposite trend dominates during years characterized by cooler Arctic waters. The detection of both IP<sub>25</sub> and % quartz throughout the record suggests that sea ice has been a persistent feature at this location of the NIS over the last millennium, even during intervals when elevated % calcite and triene Z suggest an increased influence of warmer Atlantic waters. We interpret the reduction of diene II and IP<sub>25</sub> at ~1170-1290 CE and 1880 CE-present to reflect diminished seasonal sea ice because of higher concentrations of triene Z

at the same time. In contrast, the reduction of diene II and IP<sub>25</sub> from 1450-1650 CE likely reflects a period of thick, perennial sea ice as triene Z was mostly undetectable (Fig. 3c-e).

#### 4.2.3. *Glycerol dibiphytanyl glycerol tetraethers (GDGTs)*

Changes in the degree of cyclization (number of cyclopentane moieties) in GDGTs have classically been interpreted to represent a physiological response of marine ammonia oxidizing Thaumarchaeota to changes in *in situ* temperature (e.g., Schouten et al., 2002).

Thus, the TEX<sub>86</sub> paleothermometer index has been empirically linked to annual or winter subT (0-200 m depth) in global data sets (Schouten et al., 2002; Kim et al., 2010, 2012).

This presumption is supported by a recent study along a latitudinal transect in the western Atlantic Ocean, which demonstrated that the most likely water depths where GDGTs are produced from and exported to marine sediment is around 80-250 m (Hurley et al., 2018),

similar to evidence for archaea abundance maxima at 200 m depths in the Pacific Ocean (Karner et al., 2001). Considering that Thaumarchaeota are chemolithoautotrophs that

perform ammonia oxidation (conversion of NH<sub>4</sub><sup>+</sup> to NO<sub>2</sub><sup>-</sup>), they are typically more abundant around the primary NO<sub>2</sub><sup>-</sup> maximum near the base of the photic zone (Francis et

al., 2005; Church et al., 2010; Hurley et al., 2018), and are thus most productive when there

is minimized phytoplanktic competition over NH<sub>4</sub><sup>+</sup> (Schouten et al., 2013). In the case of

the Arctic region, the latter occurs during the less productive winter months when photosynthesis for sea surface species is inhibited, which may explain the seasonal winter

temperature bias of GDGTs previously observed in this region (Rodrigo-Gámiz et al.,

2015). However, in addition to subT, recent studies have shown that several other

environmental and geochemical factors can influence the degree of cyclization, such as

growth phase (Elling et al., 2014), ammonia oxidation rates (Hurley et al., 2016), and

oxygen concentrations (Qin et al., 2015). In contrast to some other marine temperature proxies, such as the  $\delta^{18}\text{O}$  of planktic foraminifera, GDGTs do not seem to be influenced by variations in salinity (Wuchter et al., 2004, 2005; Elling et al., 2015). Finally, GDGTs appear to be relatively resistant to oxic degradation (Schouten et al., 2004), and thus, likely reflect original living conditions once deposited in the sedimentary record.

GDGTs were present above the detection limits in all marine sediment core samples, and substantially increase in concentration at the core top (Supplement Fig S1). The calculated  $\text{TEX}_{86}^{\text{L}}$  index ranged from -0.71 to -0.63 (Fig. 3f). The record displays high variability and a rather constant first order trend towards the present, in addition to the occurrence of two intervals of substantial decreases in  $\text{TEX}_{86}^{\text{L}}$  values during 1350-1530 CE and 1745-1975 CE. Both periods are preceded by periods of relatively higher  $\text{TEX}_{86}^{\text{L}}$  values during 1110-1350 CE and 1530-1745 CE, respectively. A full paleoceanographic interpretation of the  $\text{TEX}_{86}^{\text{L}}$  results is provided in the discussion.

#### 4.3. Local Icelandic $\text{TEX}_{86}^{\text{L}}$ calibration

GDGTs were also detected and above detection limits in all B997 marine surface sediments samples (n=11, Supplemental Fig S2).  $\text{TEX}_{86}^{\text{L}}$  values of these samples ranged from -0.72 to -0.61 (Table 2). The 10 marine surface sediment samples from Rodrigo-Gámiz et al. (2015) span a greater geographical and environmental range around Iceland, and hence exhibit a greater range of  $\text{TEX}_{86}^{\text{L}}$  values (-0.71 to -0.49, Table 2). When we use the combined set of Icelandic marine surface sediment samples (n=21), the regression analysis demonstrates that the integration of winter temperatures from the top 200 m of the water column provides the best regression coefficients ( $R^2=0.73$ ,  $p<0.001$ ) compared to the

integration of other seasonal temperatures and the mean annual value (Figs. 4). Thus, sedimentary values around Iceland most likely represent winter subT that integrate a signal of the uppermost 200 m of the water column, consistent with the findings of Rodrigo-Gámiz et al. (2015).

## 5. Discussion

### 5.1. Local Icelandic $\text{TEX}_{86}^L$ vs. regional Arctic calibration

If we supplement the combined Icelandic data set with more marine surface sediment samples from the greater northern North Atlantic region (Kim et al., 2010), the correlation coefficients of our winter subT (0-200 m) regression is substantially reduced ( $R^2 = 0.43$  vs. 0.73, Supplemental Fig S3). This suggests that a local Icelandic calibration is optimal over larger regional calibrations, and perhaps, more accurately captures the nuances of local Icelandic oceanography. We hypothesize that the poorer performance of a more regional GDGT calibration for the North Atlantic region may relate to the inclusion of: 1) surface sediment samples from distal locations that feature different oceanographic environments than Iceland (e.g., Hudson Bay), and/or 2) samples from higher latitude (e.g., Svalbard and the Barents Sea) that are less “responsive” in terms of GDGT cyclization as they fall under the colder end of the spectrum in the global  $\text{TEX}_{86}^L$  calibration, which is characterized by a higher uncertainty and deviation from linearity (Kim et al., 2010). The standard error in our Icelandic winter subT calibration for 0-200 m ( $\pm 0.4$  °C), is also an order of magnitude lower than the error derived from global low temperature calibrations (e.g., 4.0 °C, Kim et al., 2010; 2.8 °C, Kim et al., 2012). The reduced uncertainty achieved in our Icelandic calibration highlights the growing need for the continued development and application of

regional calibrations in future biomarker-based paleoclimate reconstructions (e.g., [Kaiser et al., 2015](#); [Foster et al., 2016](#); [Russell et al., 2018](#)). This is particularly important in areas where the temperature relationship of GDGTs deviates from the overall linear correlation observed in global calibrations (i.e., cold and warm regions).

Despite the reduced uncertainty compared to global calibrations, the regression coefficient for the Icelandic winter subT calibration ( $R^2=0.73$ ) is comparatively lower than the global calibration ( $R^2=0.86-0.87$ ; [Kim et al., 2010, 2012](#)). We hypothesize that the unconstrained confounding influence of ammonia-oxidation on the degree of GDGT cyclization (e.g., [Hurley et al., 2016](#)) may contribute to the scatter of our dataset (Fig. 4b). Although specific ammonia ( $\text{NH}_4^+$ ) and nitrite ( $\text{NO}_2^-$ ) information for this region is currently unavailable, reduced (enhanced) ammonia oxidation rates in the water column throughout the year would result in increased (decreased) degree of cyclization, thus yielding higher and lower temperatures, respectively ([Hurley et al., 2016](#)). If ammonia oxidation rates are driven by changes in ammonia supply and utilization (e.g., reduced nutrient availability in Arctic waters, or competition with phytoplankton), we cannot separate the influence of nutrient variability on the Icelandic  $\text{TEX}_{86}^{\text{L}}$  values with our current dataset. While oxygen availability has also been shown to influence the degree of cyclization in GDGTs ([Qin et al., 2015](#)), this factor is unlikely to affect the distribution of GDGTs around Iceland as these waters are relatively well-mixed and ventilated today ([Stefánsson & Ólafsson, 1991](#)), and presumably have been since the early Holocene ([Kristjánsdóttir et al., 2016](#)). With all known controlling factors considered, we suggest that our local  $\text{TEX}_{86}^{\text{L}}$  calibration improves the temperature estimates for Icelandic winter

subsurface waters. Future work in constraining the effects of ammonia-oxidation around Iceland would undoubtedly benefit the application of TEX<sub>86</sub> on the NIS.

By applying temperature calibrations to our down core TEX<sub>86</sub><sup>L</sup> record, our data reveal rapid and abrupt temperature variability on the NIS during the last millennium (Fig. 5). If the existing annual SST (Kim et al., 2010) and annual subT TEX<sub>86</sub><sup>L</sup> calibrations developed for polar regions (Kim et al., 2012) are applied, the GDGT distributions suggest that subT fluctuated up to 5 °C over the course of decades. These observations are considerably higher than expected, especially given that they are comparable to the magnitude of SST changes observed in other NIS proxy records over the entire Holocene (e.g., Andersen et al., 2004; Bendle & Rosell-Melé, 2007; Jiang et al., 2015; Kristjánsdóttir et al., 2016). As originally hypothesized, this exercise demonstrates that global calibrations that feature greater uncertainty for low temperatures and that do not include sites proximal to Iceland are not appropriate for the NIS. In contrast, by applying our local winter subT calibration, the magnitude of estimated subT is not only reduced to ranges more comparable to other proxy records for the last millennium but, importantly, also captures the modern instrumental winter subT (within calibration uncertainty) at the B997-316 GGC site (4 °C, Fig. 5), further reinforcing the application of our local Icelandic TEX<sub>86</sub><sup>L</sup> calibration.

## 5.2. NIS surface and subsurface climate variability during the Little Ice Age

The NIS represents one of the few global examples where paleo-IP<sub>25</sub> abundance in marine cores has been calibrated against observational and documentary records (Massé et al., 2008; Andrews et al., 2009b). As a result, the variability of IP<sub>25</sub> has been routinely applied

to marine sediment around Iceland as a robust indicator for seasonal sea ice (Massé et al., 2008; Andrews et al., 2009b; Sicre et al., 2013; Cabedo-Sanz et al., 2016a). Similar to these previous studies, IP<sub>25</sub> concentrations in B997-316 GGC increase abruptly during the 13<sup>th</sup> century, and with the exception of the period 1450-1650 CE, remain elevated until the 19<sup>th</sup> century when concentrations begin to diminish (Fig. 6a). By employing statistical analyses on IP<sub>25</sub> abundances and 11 other marine climate proxy datasets from marine sediment core MD99-2263, Andrews et al. (2009b) showed that a major regime shift in the marine climate off NW Iceland commenced after 1200 CE, possibly linked to a strengthening high-pressure ridge over Greenland in winter/spring that favored stronger north/northwesterly winds and increased drift ice export to Iceland. Our mineral and HBI records consistently reflect major shifts in surface conditions at a similar time and in the same direction (Fig. 3a-e), reinforcing the observed regime shift in marine climate, and increase of sea ice in particular, during the 13<sup>th</sup> century (Bergthórsson, 1969; Ogilvie & Jónsson, 2001; Massé et al., 2008; Andrews et al., 2009b; Sicre et al., 2013; Cabedo-Sanz et al., 2016a). The consistency of our surface productivity and sea ice proxy records in reflecting the established understanding of marine climate over the last millennium on the NIS supports the fidelity of the B997-316 GGC marine sediment record, and therefore, the interpretation of the GDGT record.

When the GDGT record is converted to winter subT, two pronounced centennial-scale cold anomalies exhibit mean winter subT below the record average of 4.34 °C; at 1350-1530 CE (3.99 °C) and at 1745-1975 CE (4.19 °C). These two cold anomalies are consistent with low surface productivity (% calcite and triene Z) and increased seasonal sea ice (% quartz, diene II, IP<sub>25</sub>), which suggest greater dominance of colder Arctic surface

waters between ~1250 and 1900 CE (Fig. 6a-b). In addition, alkenone-derived SST from marine core MD99-2275 50 km to the east (Fig. 1a) document steady cooling throughout this interval (Fig. 6c, [Sicre et al., 2011](#)), further supporting the presence of cool, Arctic surface waters in the vicinity of B977-316 at this time. However, the timing for the onset (1350 CE) and termination (1975 CE) of LIA cooling observed in the subsurface during winter appears to lag that of the surface (1250 and 1900 CE, respectively) (Fig. 6). A variety of model and data-based studies have demonstrated that the LIA was triggered by a combination of sustained stratospheric volcanic sulfate injection ([Zhong et al., 2010](#); [Miller et al., 2012](#); [Sicre et al., 2013](#); [Slawinska & Robock, 2018](#)), low total solar irradiance ([Shindell et al., 2001](#)) and changes in the North Atlantic Oscillation, one of the major modes of internal climate variability in the North Atlantic ([Trouet et al., 2009](#)). On the NIS, these radiative forcings directly impact the ocean surface, as manifested in the immediate and abrupt increase in seasonal sea ice, reduced northward heat transport and suppression of SSTs ([Miller et al., 2012](#)). The phase relationship between the B997-316 GGC surface proxies and GDGTs suggests that it may have taken up to a century for the radiative forcing in contact with the surface to propagate to the subsurface.

The subsurface warming observed between the two subsurface cold anomalies (~1530-1745 CE, Fig. 6d) may suggest a reduced influence of the colder Arctic water mass that generally characterized the LIA. However, similar to our surface proxies (Fig. 6a-b) and the alkenone-derived SST from MD99-2275 (Fig. 6c), a local sclerochronological  $^{14}\text{C}$  record ( $\Delta R_{\text{shell}}$ ) constructed from mollusk shells reflects the continued dominance of older Arctic waters in the benthos as well (Fig. 6e, [Wanamaker et al., 2012](#)). In fact, between 1450-1650 CE, the combination of our IP<sub>25</sub> and triene Z datasets suggest thicker and more



permanent sea ice above the B997-316 site (Fig. 6a-b), an interpretation supported by additional LIA sea ice proxy (IP<sub>25</sub> and quartz) records from the NIS (Massé et al., 2008; Andrews et al., 2009b; Cabedo-Sanz et al., 2016a). If thick sea ice conditions are maintained throughout the year, the insulating effects of sea ice would warm the subsurface waters during winter, as reflected by our GDGT record (Fig. 6d). The thickening of sea ice that we observe at 1450 CE coincides with the local intensification of LIA terrestrial cooling manifested in the synchronous advance of local Icelandic ice caps (Larsen et al., 2011; Harning et al., 2016a), and reduced Icelandic lake productivity (Geirsdóttir et al., 2013, 2019; Harning et al., 2018). A previous data-modeling comparison showed that this LIA intensification was likely forced by another episode of high stratospheric sulfate loading from explosive tropical volcanism and sustained by sea-ice/ocean feedbacks that reflected incoming solar radiation during summer (Miller et al., 2012). We suggest that the winter sea ice insulation may be another important component of the sea-ice/ocean feedback to consider in the non-linear nature of Little Ice Age cooling around Iceland.

Following the dissipation of thick sea ice conditions at 1650 CE, rising IP<sub>25</sub> and triene Z concentrations suggest the return to seasonal sea ice conditions that favored the co-productivity of sea ice and open water algae at the B997-316 site (Fig. 6a-b). The change in sea ice conditions is the likely mechanism for the return of lower subT at 1745 CE, inferred from low GDGT temperature anomalies (Fig. 6d). We hypothesize that as the sea ice thinned out during spring months, possibly spurred by the previously stored subsurface heat, the winter ice pack would have also thinned accordingly. Consequently, a more open winter sea ice pack would have facilitated increased heat flux from the ocean to the colder overlying atmosphere, as reflected by the lower GDGT-based subsurface temperatures.

573

## 574 **6. Conclusion**

575 Consistent with the community’s growing comprehension of GDGT-based temperature  
576 records at high latitudes, we show that archaeal isoprenoid GDGT distributions ( $\text{TEX}_{86}^{\text{L}}$ )  
577 around Iceland predominately reflect winter subsurface temperatures (0-200 m).  
578 Furthermore, by developing a local calibration based on a network of surface sediment  
579 samples, reconstructed NIS subsurface temperature estimates and uncertainty are improved  
580 upon those obtained from regional and global calibrations. Our  $\text{TEX}_{86}^{\text{L}}$  subsurface  
581 paleotemperature record from the NIS captures the cooling likely associated with the LIA  
582 (1250-1900 CE), as seen in additional surface proxies (sea ice and marine productivity)  
583 from the same sediment core. However, the LIA onset, intensification, and termination of  
584 the subsurface lags those changes of the surface, suggesting that it may have up to a century  
585 for changes at the surface to propagate to the subsurface during the late Holocene. We  
586 propose that the development of thick sea ice conditions during the intensification of the  
587 LIA around 1450 CE insulated the subsurface in winter, resulting in apparently warmer  
588 seasonal subsurface waters. This mechanism likely represents another seasonal component  
589 of the sea-ice/ocean feedback to be considered in the abrupt cooling manifested in and  
590 around Iceland during the LIA.

591

## 592 **Acknowledgements**

593 We kindly thank the captain, crew, and scientific staffs of the 1997 *Bjarni Sæmundsson*  
594 (B997) cruise for their considerable assistance in obtaining marine sediment cores and  
595 surface samples. The B997 cruise was principally supported by the Marine Research

Institute of Iceland, with the University of Colorado's participation supported by NSF grant #ATM-9531397. Biomarker analyses were supported by internal CU funding awarded to JS and a grant from the CU Retired Faculty Association to JTA. DJH has been supported by an Icelandic Center for Research (RANNÍS) Doctoral Student Grant #163431051. PCS and STB acknowledge support from the RANNÍS Grant of Excellence #141573052 awarded to ÁG and GHM. We greatly appreciate comments from two anonymous reviewers and the editor (Stephen Barker) that improved the overall quality and clarity of the manuscript. All data can be found online through the PANGAEA Data Publisher.

## References

- Andersen, C., Koç, N., Jennings, A.E., & Andrews, J.T. (2004). Nonuniform response of the major surface currents in the Nordic Seas to insolation forcing: Implications for the Holocene climate variability. *Paleoceanography*, 19, 1-16.
- Anderson, L.S., Flowers, G.E., Jarosch, A.H., Aðalgeirsdóttir, G.Th., Geirsdóttir, Á., Miller, G.H., Harning, D.J., Thorsteinsson, T., Magnússon, E., & Pálsson, F., (2018). Holocene glacier and climate variations in Vestfirðir, Iceland, from the modeling of Drangajökull ice cap. *Quaternary Science Reviews*, 190, 39-56.
- Andrews, J.T. (2009). Seeking a Holocene drift ice proxy: non-clay mineral variations from the SW to N-central Iceland shelf: trends, regime shifts, and periodicities. *Journal of Quaternary Science*, 24, 664-676.
- Andrews, J.T., Belt, S.T., Ólafsdóttir, S., Massé, G., & Vare, L.L. (2009b). Sea ice and marine climate variability for NW Iceland/Denmark Strait over the last 2000 cal. yr BP. *The Holocene*, 19, 775-784.
- Andrews, J.T., Darby, D.A., Eberl, D.D., Jennings, A.E., Moros, M., & Ogilvie, A. (2009a). A robust multi-site Holocene history of drift ice off northern Iceland: Implications for North Atlantic climate. *The Holocene* 19, 71-78.
- Andrews, J.T., & Eberl, D.D. (2007). Quantitative mineralogy of surface sediments on the Iceland shelf, and application to down-core studies of Holocene ice-rafted sediments. *Journal of Sedimentary Research*, 77, 469-479.

- Andrews, J.T., Hardardóttir, J., Geirsdóttir, Á., Helgadóttir, G., (2002). Late Quaternary ice extent and glacial history from the Djúpáll trough, off Vestfirðir peninsula, north-west Iceland: a stacked 36 cal. Ky environmental record. *Polar Research*, 21, 211-226.
- Andrews, J.T., Helgadóttir, G., Geirsdóttir, Á., & Jennings, A.E. (2001). Multicentury-scale records of carbonate (hydrographic?) variability on the N. Iceland margin over the last 5000 yrs. *Quaternary Research*, 56, 199-206.
- Andrews, J.T., Jónsdóttir, I., & Geirsdóttir, Á. (2018). Tracking Holocene drift-ice limits on the NW/SW Iceland shelf: comparing proxy data with observation and historical evidence. *Arctic, Antarctic, and Alpine Research*, *in press*.
- Axford, Y., Andresen, C.S., Andrews, J.T., Belt, S.T., Geirsdóttir, Á., Massé, G., Miller, G.H., Ólafsdóttir, S., & Vare, L.L. (2011). Do paleoclimate proxies agree? A test comparing 19 late Holocene climate and sea-ice reconstructions from Icelandic marine and lake sediments. *Journal of Quaternary Science*, 26, 645-656.
- Belkin, I.M., Cornillon, P.C., & Sherman, K. (2009). Fronts in large marine ecosystems. *Progress in Oceanography*, 81, 223-236.
- Belt, S.T. (2018). Source-specific biomarkers as proxies for Arctic and Antarctic sea ice. *Organic Geochemistry*, 125, 277-298.
- Belt, S.T., Allard, W.G., Massé, G., Robert, J.-M., & Rowland, S.J. (2000). Highly branched isoprenoids (HBIs): Identification of the most common and abundant sedimentary isomers. *Geochimica and Cosmochimica Acta*, 64, 3839-3851.
- Belt, S.T., Brown, T.A., Navarro Rodriguez, A., Cabedo Sanz, P., Tonkin, A., & Ingle, R. (2012). A reproducible method for the extraction, identification and quantification of the Arctic sea ice proxy IP<sub>25</sub> from marine sediments. *Analytical Methods*, 4, 704-713.
- Belt, S.T., Brown, T.A., Smik, L., Assmy, P., & Mundy, C.J. (2018). Sterol identification in floating Arctic sea ice algal aggregates and the Antarctic sea ice diatom *Berkeleya adeliensis*. *Organic Geochemistry*, 118, 1-3.
- Belt, S.T., Brown, T.A., Smik, L., Tatarek, A., Wiktor, J., Stowasser, G., Assmy, P., Allen, C.S., & Husum, K. (2017). Identification of C<sub>25</sub> highly branched isoprenoid (HBI) alkenes in diatoms of the genus *Rhizosolenia* in polar and sub-polar marine phytoplankton. *Organic Geochemistry*, 110, 65-72.
- Belt, S.T., Brown, T.A., Ringrose, A.E., Cabedo-Sanz, P., Mundy, C.J., Gosselin, M., & Poulin, M. (2013). Quantitative measurement of the sea ice diatom biomarker IP<sub>25</sub> and sterols in Arctic sea ice and underlying sediments: Further considerations for palaeo sea ice reconstructions. *Organic Geochemistry*, 62, 33-45.

- Belt, S.T., Cabedo-Sanz, P., Smik, L., Navarro-Rodriguez, A., Berben, S.M.P., Knies, J., & Husum, K. (2015). Identification of paleo Arctic winter sea ice limits and the marginal ice zone: Optimised biomarker-based reconstructions of late Quaternary Arctic sea ice. *Earth and Planetary Science Letters*, 431, 127-139.
- Belt, S.T., Massé, G., Rowland, S.J., Poulin, M., Michel, C., & LeBlanc, B. (2007). A novel chemical fossil of palaeo sea ice: IP<sub>25</sub>. *Organic Geochemistry*, 38, 16-27.
- Belt, S.T., Massé, G., Vare, L.L., Rowland, S.J., Poulin, M., Sicre, M.-A., Sampei, M., & Fortier, L. (2008). Distinctive <sup>13</sup>C isotopic signature distinguishes a novel sea ice biomarker in Arctic sediments and sediment traps. *Marine Chemistry*, 112, 158-167.
- Belt, S.T., & Müller, J. (2013). The Arctic sea ice biomarker IP<sub>25</sub>: a review of current understanding, recommendations for future research and applications in palaeo sea ice reconstructions. *Quaternary Science Reviews*, 79, 9-25.
- Belt, S.T., Smik, L., Brown, T.A., Kim, J.-H., Rowland, S.J., Allen, C.S., Gal, J.-K., Shin, K.-H., Lee, J.I., & Taylor, K.W.R. (2016). Source identification and distribution reveals the potential of the geochemical Antarctic sea ice proxy IPSO<sub>25</sub>. *Nature Communications*, 7, 1-10.
- Bendle, J.A.P., & Rosell-Melé, A. (2007). High-resolution alkenone sea surface temperature variability on the North Icelandic Shelf: implications for Nordic Seas palaeoclimatic development during the Holocene. *The Holocene*, 17, 9-24.
- Bergthórsson, P. (1969). An estimate of drift ice and temperature in Iceland in 1000 years. *Jökull*, 19, 94-101.
- Blaauw, M. (2010). Methods and code for ‘classical’ age-modeling of radiocarbon sequences. *Quaternary Geochronology*, 5, 512-518.
- Brown, T.A., Belt, S.T., Tatarek, A., & Mundy, C.J. (2014). Source identification of the Arctic sea ice proxy IP<sub>25</sub>. *Nature Communications*, 5, 4197.
- Brynjólfsson, S., Schomacker, A., Ingólfsson, Ó., & Keiding, J.K. (2015a). Cosmogenic <sup>36</sup>Cl exposure ages reveal a 9.3 ka BP glacier advance and the Late Weichselian-Early Holocene glacial history of the Drangajökull region, northwest Iceland. *Quaternary Science Reviews*, 126, 140-157.
- Buckley, M.W., & Marshall, J. (2016). Observations, inferences, and mechanisms of the Atlantic Meridional Overturning Circulation: A review. *Journal of Geophysics*, 54, 5-63.
- Cabedo-Sanz, P., Belt, S.T., Jennings, A.E., Andrews, J.T., & Geirsdóttir, Á. (2016a). Variability in drift ice export from the Arctic Ocean to the North Icelandic Shelf over the last 8000 years: A multi-proxy evaluation. *Quaternary Science Reviews*, 146, 99-115.

- Cabedo-Sanz, P., Belt, S.T., Knies, J., & Husum, K. (2013). Identification of contrasting seasonal sea ice conditions during the Younger Dryas. *Quaternary Science Reviews*, 79, 74-86.
- Cabedo-Sanz, P., Smik, L., & Belt, S.T. (2016b). On the stability of various highly branched isoprenoid (HBI) lipids in stored sediments and sediment extracts. *Organic Geochemistry*, 97, 74-77.
- Caesar, L., Rahmstorf, S., Robinson, A., Feulner, G., & Saba, V. (2018). Observed fingerprint of a weakening Atlantic Ocean overturning circulation. *Nature*, 556, 191-198.
- Castañeda, I.S., Smith, L.M., Kristjánssdóttir, G.B., & Andrews, J.T. (2004). Temporal changes in Holocene  $\delta^{18}\text{O}$  records from northwest and central North Iceland Shelf. *Journal of Quaternary Science*, 19, 321-334.
- Chivall, D., M'Boule, D., Sinke-Schoen, D., Sinninghe Damsté, J.S., Schouten, S., & van der Meer, M.T.J. (2014). Impact of salinity and growth phase on alkenone distributions in coastal haptophytes. *Organic Geochemistry*, 67, 31-34.
- Church, M.J., Wai, B., Karl, D.M., & DeLong, E.F. (2010). Abundances of crenarchaeal amoA genes and transcripts in the Pacific Ocean. *Environmental Microbiology*, 12, 679-688.
- Collins, L.G., Allen, C.S., Pike, J., Hodgson, D.A., Weckström, K., & Massé, G. (2013). Evaluating highly branched isoprenoid (HBI) biomarkers as a novel Antarctic sea-ice proxy in deep ocean glacial age sediments. *Quaternary Science Reviews*, 79, 87-98.
- Darby, D.A., Andrews, J.T., Belt, S.T., Jennings, A.E., & Cabedo-Sanz, P. (2017). Holocene cyclic records of ice-rafted debris and sea ice variations on the East Greenland and Northwest Iceland margins. *Arctic, Antarctic, and Alpine Research*, 49, 649-672.
- Denton, G.H., & Broecker, W.S. (2008). Wobbly ocean conveyor circulation during the Holocene? *Quaternary Science Reviews*, 27, 1939-1950.
- Divine, D.V., & Dick, C. (2007). March through August Ice Edge Positions in the Nordic Seas, 1750-2002, Version 1. Boulder, Colorado USA. *NSIDC: National Snow and Ice Data Center*.
- Eberl, D.D. (2003). *User guide to RockJock: A program for determining quantitative mineralogy from X-ray diffraction data*. United States Geological Survey, Open File Report 03-78, 40 pp, Washington, DC.
- Eiríksson, J., Larsen, G., Knudsen, K.L., Heinemeier, J., & Símonarson, L.A. (2004). Marine reservoir age variability and water mass distribution in the Iceland Sea. *Quaternary Science Reviews*, 23, 2247-2268.



- 769 Elling, F.J., Könneke, M., Lipp, J.S., Becker, K.W., Gagen, E.J., & Hinrichs, K.-U. (2014).  
770 Effects of growth phase on the membrane lipid composition of the thaumarchaeon  
771 *Nitrosopumilus maritimus* and their implications for archaeal lipid distributions in the  
772 marine environment. *Geochimica et Cosmochimica Acta*, 141, 579-597.
- 773  
774 Elling, F.J., Könneke, M., Mußmann, M., Greve, A., & Hinrichs, K.-U. (2015). Influence  
775 of temperature, pH, and salinity on membrane lipid composition and TEX<sub>86</sub> of marine  
776 planktonic thaumarchaeal isolates. *Geochimica et Cosmochimica Acta*, 171, 238-255.
- 777  
778 Foster, L.C., Pearson, E.J., Juggins, S., Hodgson, D.A., Saunders, K.M., Verleyen, E., &  
779 Roberts, S.J. (2016). Development of a regional glycerol dialkyl glycerol tetraether  
780 (GDGT)-temperature calibration for Antarctic and sub-Antarctic lakes. *Earth and*  
781 *Planetary Science Letters*, 433, 370-379.
- 782  
783 Francis, C.A., Roberts, K.J., Beman, J.M., Santoro, A.E., & Oakley, B.B. (2005). Ubiquity  
784 and diversity of ammonia-oxidizing archaea in water columns and sediments of the ocean.  
785 *Proceedings of the National Academy of Sciences*, 102, 14683-14688.
- 786  
787 Geirsdóttir, Á., Miller, G.H., Andrews, J.T., Harning, D.J., Anderson, L.S., Larsen, D.J.,  
788 Florian, C. & Thordarson, T. (2019). The onset of Neoglaciation in Iceland and the 4.2 ka  
789 event. *Climate of the Past Discussions*, 14, 25-40.
- 790  
791 Geirsdóttir, Á., Miller, G.H., Larsen, D.J., & Ólafsdóttir, S. (2013). Abrupt Holocene  
792 climate transitions in the northern North Atlantic region recorded by synchronized  
793 lacustrine records in Iceland. *Quaternary Science Reviews*, 70, 48-62.
- 794  
795 Geirsdóttir, Á., Miller, G.H., Thordarson, T., & Ólafsdóttir, K.B. (2009). A 2000 year  
796 record of climate variations reconstructed from Haukadalsvatn, West Iceland. *Journal of*  
797 *Paleolimnology*, 41, 95-115.
- 798  
799 Giraudeau, J., Jennings, A.E., & Andrews, J.T. (2004). Timing and mechanisms of surface  
800 and intermediate water circulation changes in the Nordic Sea over the last 10000 cal years:  
801 A view from the North Iceland Shelf. *Quaternary Science Reviews*, 23, 2127-2139.
- 802  
803 Hall, I.R., Bianchi, G.G., & Evans, J.R. (2004). Centennial to millennial scale Holocene  
804 climate-deep water linkage in the North Atlantic. *Quaternary Science Reviews*, 23, 1529-  
805 1536.
- 806  
807 Harning, D.J., Geirsdóttir, Á., Miller, G.H., & Anderson, L. (2016a). Episodic expansion  
808 of Drangajökull, Vestfirðir, Iceland over the last 3 ka culminating in its maximum  
809 dimension during the Little Ice Age. *Quaternary Science Reviews*, 152, 118-131.
- 810  
811 Harning, D.J., Geirsdóttir, Á., Miller, G.H., & Zalzal, K. (2016b). Early Holocene  
812 deglaciation of Drangajökull, Vestfirðir, Iceland. *Quaternary Science Reviews*, 153, 192-  
813 198.
- 814

- Harning, D.J., Geirsdóttir, Á., & Miller, G.H. (2018). Punctuated Holocene climate of Vestfirðir, Iceland, linked to internal/external variables and oceanographic conditions. *Quaternary Science Reviews*, 189, 31-42.
- Helgadóttir, G. (1997). Paleoclimate (0 to >14 ka) of W and NW Iceland: an Iceland/USA contribution to P.A.L.E. Cruise Report B9-97 R/V Bjarni Sæmundsson RE 30 17<sup>th</sup>-30<sup>th</sup> July 1997. No. 62, *Marine Research Institute of Iceland*, Reykjavík, Iceland.
- Herfort, L., Schouten, S., Boon, J.P., & Sinninghe Damsté, J.S. (2006). Application of TEX<sub>86</sub> temperature proxy to the southern North Sea. *Organic Geochemistry*, 37, 1715-1726.
- Hopkins, T.S. (1991). The GIN Sea – A synthesis of its physical oceanography and literature review 1972-1985. *Earth Science Reviews*, 30, 175-318.
- Hopmans, E.C., Schouten, S., & Sinninghe Damsté, J.S. (2016). The effect of improved chromatography on GDGT-based palaeoproxies. *Organic Geochemistry*, 93, 1-6.
- Huang, W.-Y., & Meinschein, W. (1976). Sterols as ecological indicators. *Geochimica et Cosmochimica Acta*, 43, 739-745.
- Huguet, C., Hopmans, E.C., Febo-Ayala, W., Thompson, D.H., Sinninghe Damsté, J.S., & Schouten, S. (2006). An improved method to determine the absolute abundance of glycerol dibiphytanyl glycerol tetraether lipids. *Organic Geochemistry*, 37, 1036-1041.
- Hurley, S.J., Elling, F.J., Könneke, M., Buchwald, C., Wankel, S.D., Santoro, A.E., Lipp, J.S., Hinrichs, K.-U., & Pearson, A. (2016). Influence of ammonia oxidation rate on thaumarchaeal lipid composition and the TEX<sub>86</sub> temperature proxy. *Proceedings of the National Academy of Sciences*, 113, 7762-7767.
- Hurley, S.J., Lipp, J.S., Close, H.G., Hinrichs, K.-U., & Pearson, A. (2018). Distribution and export of isoprenoid tetraether lipids in suspended particulate matter from the water column of the Western Atlantic Ocean. *Organic Geochemistry*, 116, 90-102.
- Jiang, H., Muscheler, R., Björck, S., Seidenkrantz, M.-S., Olsen, J., Sha, L., Sjolte, J., Eiríksson, J., Ran, L., Knudsen, K.-L., & Knudsen, M.F. (2015). Solar forcing of Holocene summer sea-surface temperatures in the northern North Atlantic. *Geology*, 43, 2-5.
- Justwan, A., Koc, N., & Jennings, A.E. (2008). Evolution of the Irminger and East Icelandic Current systems through the Holocene, revealed by diatom-based sea surface temperature reconstructions. *Quaternary Science Reviews*, 27, 1571-1582.
- Kaiser, J., Schouten, S., Kilian, R., Arz, H.W., Lamy, F., & Sinninghe Damsté, J.S. (2015). Isoprenoid and branched GDGT-based proxies for surface sediments from marine, fjord and lake environments in Chile. *Organic Geochemistry*, 89-90, 117-127.



- 861 Karner, M.B., DeLong, E.F., & Karl, D.M. (2001). Archaeal dominance in the mesopelagic  
862 zone of the Pacific Ocean. *Nature*, 409, 507-510.
- 863
- 864 Kim, J.-H., van der Meer, J., Schouten, S., Helmke, P., Willmott, V., Sangiorgi, F., Koç,  
865 N., Hopmans, E. C., & Sinninghe Damsté, J. S. (2010). New indices and calibrations  
866 derived from the distribution of crenarchaeal isoprenoid tetraether lipids: Implications for  
867 past sea surface temperature reconstructions. *Geochimica et Cosmochimica Acta*, 74,  
868 4639–4654.
- 869
- 870 Kim, J.-H., Crosta, X., Willmott, V., Renssen, H., Bonnin, J., Helmke, P., Schouten, S., &  
871 Sinninghe Damsté, J.S. (2012). Holocene subsurface temperature variability in the eastern  
872 Antarctic continental margin. *Geophysical Research Letters*, 39, 3-8.
- 873
- 874 Knudsen, K.L., Eirikson, J., Jansen, E., Jiang, H., Rytter, F., & Gudmundsdottir, E.R.  
875 (2004). Paleoceanographic changes off North Iceland through the last 1200 yrs:  
876 foraminifera, stable isotopes, diatoms and ice rafted debris. *Quaternary Science Reviews*,  
877 23, 2231-2246.
- 878
- 879 Köseoğlu, D., Belt, S.T., Smik, L., Yao, H., Panieri, G., & Knies, J. (2018).  
880 Complementary biomarker-based methods for characterizing Arctic sea ice conditions: A  
881 case study comparison between multivariate analysis and the PIP<sub>25</sub> index. *Geochimica et*  
882 *Cosmochimica Acta*, 222, 406-420.
- 883
- 884 Kristjánssdóttir, G.B., Moros, M., Andrews, J.T., & Jennings, A.E. (2016). Holocene  
885 Mg/Ca, alkenones, and light stable isotope measurements on the outer North Iceland shelf  
886 (MD99-2269): A comparison with other multi-proxy data and sub-division of the  
887 Holocene. *The Holocene*, 26, 1-11.
- 888
- 889 Larsen, D.J., Miller, G.H., Geirsdóttir, Á., & Thordarson, T. (2011). A 3000-year varved  
890 record of glacier activity and climate change from the proglacial lake Hvítárvatn, Iceland.  
891 *Quaternary Science Reviews*, 30, 2715-2731.
- 892
- 893 Larsen, D.J., Miller, G.H., Geirsdóttir, Á., & Ólafssdóttir, S. (2012). Non-linear Holocene  
894 climate evolution in the North Atlantic: a high-resolution, multi-proxy record of glacier  
895 activity and environmental change from Hvítárvatn, central Iceland. *Quaternary Science*  
896 *Reviews*, 39, 14-25.
- 897
- 898 Locarnini, R.A., Mishonov, A.V., Antonov, J.I., Boyer, T.P., Garcia, H.E., Baranova, O.K.,  
899 Zweng, M.M., & Johnson, D.R. (2010). *World Ocean Atlas 2009, Volume 1: Temperature*.  
900 S. Levitus, Ed. NOAA Atlas NESDIS 68, U.S. Government Printing Office, Washington,  
901 D.C., 184 pp.
- 902
- 903 Massé, G., Rowland, S.J., Sicre, M.-A., Jacob, J., Jansen, E., & Belt, S.T. (2008). Abrupt  
904 climate changes for Iceland during the last millenium: Evidence form high resolution sea  
905 ice reconstructions. *Earth and Planetary Science Letters*, 269, 565-569.
- 906

- Maykut, G.A. (1978). Energy exchange over young sea ice in the central Arctic. *Journal of Geophysical Research*, 83, 3646-3658.
- Maykut, G.A. (1982). Large-scale heat exchange and ice production in the central Arctic. *Journal of Geophysical Research*, 87, 7971-7984.
- Miller, G.H., Geirsdóttir, Á., Zhong, Y., Larsen, D.J., Otto-Bliesner, B.L., Holland, M.M., Bailey, D.A., Refsnider, K.A., Lehman, S.J., Southon, J.R., Anderson, C., Björnsson, H., & Thordarson, T. (2012). Abrupt onset of the Little Ice Age triggered by volcanism and sustained by sea-ice/ocean feedbacks. *Geophysical Research Letters*, 39, 1-5.
- Moossen, H., Bendle, J., Seki, O., Quillmann, U., & Kawamura, K. (2015). North Atlantic Holocene climate evolution recorded by high-resolution terrestrial and marine biomarker records. *Quaternary Science Reviews*, 129, 111-127.
- Moros, M., Andrews, J.T., Eberl, D.D., & Jansen, E. (2006). Holocene history of drift ice in the northern North Atlantic: Evidence for differential spatial and temporal modes. *Paleoceanography*, 21, 1-10.
- Müller, J., Wagner, A., Fahl, K., Stein, R., Prange, M., & Lohmann, G. (2011). Towards quantitative sea ice reconstructions in the northern North Atlantic: a combined biomarker and numerical modelling approach. *Earth and Planetary Science Letters*, 306, 137-148.
- Norðdahl, H., Ingólfsson, Ó., (2015). Collapse of the Icelandic ice sheet controlled by sea-level rise? *Arktos*, 13, 1-18.
- Ogilvie, A.E.J., & Jónsson, T. (2001). “Little Ice Age” research: A perspective from Iceland. *Climatic Change*, 48, 9-52.
- Ólafsdóttir, S., Jennings, A.E., Geirsdóttir, Á., Andrews, J., & Miller, G.H. (2010). Holocene variability of the North Atlantic Irminger current on the south- and northwest shelf of Iceland. *Marine micropaleontology*, 77, 101-118.
- Ólafsson, J., Ólafsdóttir, S.R., & Briem, J. (2008). Vatnsföll og vistkerfi strandsjávar. *Náttúrufræðingurinn*, 76, 95-108.
- Orme, L.C., Miettinen, A., Divine, D., Husum, K., Pearce, C., Van Nieuwenhove, N., Born, A., Mohan, R., & Seidenkrantz, M.-S. (2018). Subpolar North Atlantic sea surface temperature since 6 ka BP: Indications of anomalous ocean-atmosphere interactions at 4-2 ka BP. *Quaternary Science Reviews*, 194, 128-142.
- Orvik, K.A., Skagseth, Ø., & Mork, M. (2001). Atlantic inflow to the Nordic Seas: current structure and volume fluxes from moored current meters, VM-ADCP and SeaSoar-CTD observations, 1995-1999. *Deep-Sea Research*, 48, 937-957.

- Patton, H., Hubbard, A., Bradwell, T., Schomacker, A., (2017). The configuration, sensitivity and rapid retreat of the Late Weichselian Icelandic ice sheet. *Earth-Science Reviews*, 166, 223-245.
- Prahl, F.G., Mix, A.C., & Sparrow, M.A. (2006). Alkenone paleothermometry: Biological lessons from marine sediment records off western South America. *Geochimica et Cosmochimica Acta*, 70, 101-117.
- Qin, W., Carlson, L.T., Armbrust, E.V., Devol, A.H., Moffett, J.W., Stahl, D.A., & Ingalls, A.E. (2015). Confounding effects of oxygen and temperature on the TEX<sub>86</sub> signature of marine Thaumarchaeota. *Proceedings of the National Academy of Sciences*, 112, 10979-10984.
- Ran, L., Knudsen, K.L., & Eiríksson, J. (2008). A high-resolution Holocene diatom record on the North Icelandic Shelf. *Boreas*, 37, 399-413.
- Reimer, P.J., Bard, E., Bayliss, A., Beck, W.J., Blackwell, P.G., Brock Ramsey, C., Buck, C.E., Cheng, H., Edwards, R.L., Friedrich, M., Grootes, P.M., Guilderson, T.P., Hafliðason, H., Hajdas, I., Hatté, C., Heaton, T.J., Hoffmann, D.L., Hogg, A.G., Hughen, K.A., Kaiser, K.F., Kromer, B., Manning, S.W., Niu, M., Reimer, R.W., Richards, D.A., Scott, E.M., Southon, J.R., Staff, R.A., Turney, C.S.M., & van der Plicht, J. (2013). Intcal13 and Marine13 radiocarbon age calibration curves 0-50,000 years cal BP. *Radiocarbon*, 55, 1869-1887.
- Rodrigo-Gámiz, M., Rampen, S.W., de Haas, H., Baas, M., Schouten, S., & Sinninghe-Damsté, J.S. (2015). Constraints on the applicability of the organic temperature proxies Uk37', TEX<sub>86</sub> and LDI in the subpolar region around Iceland. *Biogeosciences*, 12, 6573-6590.
- Rowland, S.J., Allard, W.G., Belt, S.T., Massé, G., Robert, J.-M., Blackburn, S., Frampton, D., Revill, A.T., & Volkman, J.K. (2001). Factors influencing the distributions of polyunsaturated terpenoids in the diatom, *Rhizosolenia setigera*. *Phytochemistry*, 58, 717-728.
- Rueda, G., Rosell-Melé, A., Escala, M., Gyllencreutz, R., & Backman, J. (2009). Comparison of instrumental and GDGT-based estimates of sea surface and air temperatures from the Skaggeirak. *Organic Geochemistry*, 40, 287-291.
- Russell, J.M., Hopmans, E.C., Loomis, S.E., Liang, J., & Sinninghe Damsté, J.S. (2018). Distributions of 5- and 6-methyl branched glycerol dialkyl glycerol tetraethers (brGDGTs) in East African lake sediment: Effects of temperature, pH, and new lacustrine paleotemperature calibrations. *Organic Geochemistry*, 117, 56-69.
- Schouten, S., Hopmans, E.C., Schefuss, E., & Sinninghe Damsté, J.S. (2002). Distributional variations in marine crenarchaeotal membrane lipids: a new tool for

- reconstructing ancient sea water temperatures? *Earth and Planetary Science Letters*, 204, 265-274.
- Schouten, S., Hopmans, E.C., & Sinninghe Damsté, J.S. (2004). The effect of maturity and depositional redox conditions on archaeal tetraether lipid palaeothermometry. *Organic Geochemistry*, 35, 567-571.
- Schouten, S., Hopmans, E.C., & Sinninghe Damsté, J.S. (2013). The organic geochemistry of glycerol dialkyl glycerol tetraether lipids: A review. *Organic Geochemistry*, 54, 19-61.
- Shindell, D.T., Schmidt, G.A., Mann, M.E., Rind, D., & Waple, A. (2001). Solar forcing of regional climate change during the Maunder Minimum. *Science*, 294, 2159-2152.
- Sicre, M.-A., Hall, I.R., Mignot, J., Khodri, M., Ezat, U., Truong, M.-X., Eiríksson, J., & Knudsen, K.-L. (2011). Sea surface temperature variability in the subpolar Atlantic over the last two millennia. *Paleoceanography*, 26, 1-10.
- Sicre, M.-A., Khodri, M., Mignot, J., Eiríksson, J., Knudsen, K.-L., Ezat, U., Closset, I., Nogues, P., & Massé, G. (2013). Sea surface temperature and sea ice variability in the subpolar North Atlantic from explosive volcanism of the late thirteenth century. *Geophysical Research Letters*, 40, 5526-5539.
- Slawinska, J., & Robock, A. (2018). Impact of volcanic eruptions on decadal to centennial fluctuations of Arctic sea ice extent during the last millennium and on initiation of the Little Ice Age. *Journal of Climate*, 31, 2145-2167.
- Smik, L., Cabedo-Sanz, P., & Belt, S.T. (2016). Semi-quantitative estimates of paleo Arctic sea ice concentration based on source-specific highly branched isoprenoid alkenes: A further development of the PIP<sub>25</sub> index. *Organic Geochemistry*, 92, 63-69.
- Smith, L.M., Andrews, J.T., Castañeda, I.S., Kristjánssdóttir, G.B., Jennings, A.E., & Sveinbjörnsdóttir, Á.E. (2005). Temperature reconstructions for SW and N Iceland waters over the last 10 cal ka based on  $\delta^{18}\text{O}$  records from planktic and benthic foraminifera. *Quaternary Science Reviews*, 24, 1723-1740.
- Solignac, S., Giraudeau, J., & de Vernal, A. (2006). Holocene sea surface conditions in the western North Atlantic: Spatial and temporal heterogeneities. *Paleoceanography*, 21, 1-6.
- Spielhagen, R.F., Werner, K., Sørensen, S.A., Zamelczyk, K., Kandiano, E., Budeus, G., Husum, K., Marchitto, T.M., & Hald, M. (2011). Enhanced modern heat transfer to the Arctic by warm Atlantic water. *Science*, 311, 450-453.
- Stefánsson, U. (1962). North Icelandic Waters. *Rit Fiskideildar III. Bind*, vol 3.
- Stefánsson, U. (1968). Dissolved nutrients, oxygen and water masses in the Northern Irminger Sea. *Deep-Sea Research*, 15, 541-575.

- 1043
- 1044 Stefánsson, U., & Ólafsson, J. (1991). Nutrients and fertility of Icelandic waters. *Rit*
- 1045 *fiskideildar*, 1-56.
- 1046
- 1047 Stein, R., Fahl, K., Schreck, M., Knorr, G., Niessen, F., Forwick, M., Gebhardt, C., Jensen,
- 1048 L., Kaminski, M., Kopf, A., Matthiessen, J., Jokat, W., & Lohmann, G. (2016). Evidence
- 1049 for ice-free summers in the late Miocene central Arctic Ocean. *Nature Communications*, 7,
- 1050 11148.
- 1051
- 1052 Stuiver, M., Reimer, P.J., & Reimer, R.W. (2018). CALIB 7.1 [WWW program] at
- 1053 <http://calib.org>, accessed 2018-11-16.
- 1054
- 1055 Thornalley, D.J.R., Oppo, D.W., Ortega, P., Robson, J.I., Brierley, C.M., Davis, R., Hall,
- 1056 I.R., Moffa-Sanchez, P., Rose, N.L., Spooner, P.T., Yashayaev, I., & Keigwin, L.D. (2018).
- 1057 Anomalous weak Labrador Sea convection and Atlantic overturning during the past 150
- 1058 years. *Nature*, 556, 227-232.
- 1059
- 1060 Thorndike, A.S., Rothrock, D.A., Maykut, G.A., & Colony, R. (1975). The thickness
- 1061 distribution of sea ice. *Journal of Geophysical Research*, 80, 4501-4513.
- 1062
- 1063 Tierney, J.E., Tingley, M.P., (2014). A Bayesian, spatially-varying calibration model for
- 1064 the TEX<sub>86</sub> proxy. *Geochimica et Cosmochimica Acta*, 127, 83-106.
- 1065
- 1066 Trouet, V., Esper, J., Graham, N.E., Baker, A., Scourse, J.D., & Frank, D.C. (2009).
- 1067 Persistent positive North Atlantic oscillation mode dominated the medieval climate
- 1068 anomaly. *Science*, 324, 78-80.
- 1069
- 1070 Volkman, J.K. (1986). A review of sterol markers for marine and terrigenous organic
- 1071 matter. *Organic Geochemistry*, 9, 83-99.
- 1072
- 1073 Volkman, J.K., Barrett, S.M., Blackburn, S.I., Mansour, M.P., Sikes, E.L., & Gelin, F.
- 1074 (1998). Microalgal biomarkers: a review of recent developments. *Organic Geochemistry*,
- 1075 29, 1163-1179.
- 1076
- 1077 Wanamaker, A.D., Butler, P.G., Scourse, J.D., Heinemeier, J., Eiríksson, J., Knudsen,
- 1078 K.L., & Richardson, C.A. (2012). Surface changes in the North Atlantic meridional
- 1079 overturning circulation during the last millennium. *Nature Communications*, 3, 1-7.
- 1080
- 1081 Wuchter, C., Schouten, S., Coolen, M.J.L., & Sinninghe Damsté, J.S. (2004). Temperature-
- 1082 dependent variation in the distribution of tetraether membrane lipids of marine
- 1083 Crenarchaeota: implications for TEX<sub>86</sub> paleothermometry. *Paleoceanography*, 19, 1-10.
- 1084
- 1085 Wuchter, C., Schouten, S., Wakeham, S.G., & Sinninghe Damsté, J.S. (2005). Temporal
- 1086 and spatial variation in tetraether membrane lipids of marine Crenarchaeota in particulate
- 1087 organic matter: implications for TEX<sub>86</sub> paleothermometry. *Paleoceanography* 20, 1-11.
- 1088

Wunsch, C. (1980). Meridional heat flux of the North Atlantic Ocean. *Proceedings of the National Academy of Sciences*, 77, 5043-5047.

Xiao, X., Zhao, M., Knudsen, K.L., Sha, L., Eiríksson, J., Gudmundsdóttir, E., Jiang, H., & Guo, Z. (2017). Deglacial and Holocene sea-ice variability north of Iceland and response to ocean circulation changes. *Earth and Planetary Science Letters*, 472, 14-24.

Zhai, L., Guðmundsson, K., Miller, P., Peng, W., Guðfinnsson, H., Debes, H., Hátun, H., White III, G.N., Hernández Walls, R., Sathyendranath, S., & Platt, T. (2012). Phytoplankton phenology and production around Iceland and Faroes. *Continental Shelf Research*, 37, 15-25.

Zhong, Y., Miller, G.H., Otto-Bliesner, B.L., Holland, M.M., Bailey, D.A., Schneider, D.P., & Geirsdóttir, Á. (2010). Centennial-scale climate change from decadal-paced explosive volcanism: a coupled sea ice-ocean mechanism. *Climate Dynamics*, 37, 2373-2387.

## TABLES and FIGURES (8 units):

**Table 1:** Radiocarbon information.  $^{14}\text{C}$  ages calibrated in Calib 7.1 (Stuiver et al., 2018) using the MARINE13 calibration curve (Reimer et al., 2013) and a  $\Delta R$  of 0. Note that  $^{14}\text{C}$  and calibrated ages are presented as BP (Before Present) in this table, and as CE (Common Era) in the main text.

Sediment core	Sediment depth (cm)	Lab ID	Material	$\delta^{13}\text{C}$ (‰)	Conventional $^{14}\text{C}$ date BP $\pm \sigma$	$\Delta R$	Calibrated age BP $\pm \sigma$
B997-316 SGC	7.5	GRL-1691-S	mollusk ( <i>T. equalis</i> )	0.62	294 $\pm$ 91	0	<400
B997-316 SGC	18	GRL-1690-S	mollusk ( <i>T. equalis</i> )	-7.2	402 $\pm$ 38	0	<400
B997-316 GGC	49.5	CURL-18624	foraminifera ( <i>N. labradorica</i> and <i>G. auriculata arctica</i> )	-14	1030 $\pm$ 15	0	600 $\pm$ 35
B997-316 GGC	135	CURL-19693	mollusk ( <i>T. equalis</i> )	-9	1040 $\pm$ 15	0	620 $\pm$ 25
B997-316 GGC	160	CURL-19511	mollusk ( <i>T. equalis</i> )	-8.5	1075 $\pm$ 15	0	645 $\pm$ 15
B997-316 GGC	212.5	CURL-20191	mollusk ( <i>T. equalis</i> )	-5	1245 $\pm$ 15	0	780 $\pm$ 35

**Table 2:** Surface sediment calibration information. \* indicates data from Rodrigo-Gámiz et al. (2015).

Site ID	Latitude	Longitude	Water depth (mbsl)	TEX <sub>86</sub> <sup>L</sup>
B997-313	66.617000°	-23.933000°	213	-0.67
B997-315	66.736000°	-24.332000°	217	-0.69
B997-316	66.746000°	-18.792000°	658	-0.68
B997-319	66.447000°	-18.843000°	422	-0.72
B997-324	66.527000°	-21.152000°	281	-0.65
B997-334	66.410000°	-21.880000°	112	-0.70
B997-329	65.965000°	-21.294000°	112	-0.68
B997-331	66.136000°	-21.591000°	165	-0.71
B997-344	64.836000°	-24.369000°	284	-0.61
B997-346	64.927000°	-24.129000°	320	-0.63



B997-347	63.928000°	-24.482000°	327	-0.64
Station 1*	62.000317°	-15.999183°	2255	-0.49
Station 7*	61.498550°	-24.172250°	1628	-0.51
Station 3*	63.366200°	-16.628267°	240	-0.59
Station 5*	63.583267°	-22.143733°	188	-0.62
Station 6*	63.238233°	-22.561417°	315	-0.61
Station 8*	64.293183°	-24.147083°	260	-0.62
Station 10*	66.677450°	-24.179500°	241	-0.64
Station 11*	66.633317°	-20.833433°	367	-0.63
Station 13*	67.501633°	-15.069217°	884	-0.71
Station 14*	66.303100°	-13.972817°	262	-0.68

**Fig. 1:** A) Overview maps of modern Icelandic oceanography. A) February 2014 and B) May 2014 50 m depth *in situ* temperature integrated from local CTD stations. Marine sediment cores (black dots) and used B997 surface sediment sample locations (black + and B997-316 GGC core site) are marked. C) May 2014 S-N trending cross section of NIS bathymetry and vertical *in situ* temperature structure along the Siglunes transect (A-A' in panels A and B) and through the B997-316 GGC marine sediment core site. Data from Hafrannsóknastofnun ([Marine and Freshwater Research Institute, http://www.hafro.is/Sjora/](http://www.hafro.is/Sjora/)).

**Fig. 2:** CLAM age model. Gray shaded area denotes the 95% confidence envelope (Blaauw, 2010). Teal and asterisked mollusk ages are from the adjacent short gravity core, B997-316 SGC. Radiocarbon information provided in Table 1.

**Fig. 3:** B997-316 GGC marine sediment core climate proxies over the last millennium. A) % quartz, B) % calcite, C) triene Z concentrations, D) diene II concentrations, E) IP<sub>25</sub> concentrations, and F) TEX<sub>86</sub><sup>L</sup>. Blue boxes highlight colder, LIA-like conditions reflected in the surface climate proxies (A-E) and the subsurface proxy (F).

**Fig. 4:** Regression analysis summary of surface sediment GDGT calibration. A) Correlation coefficient (R<sup>2</sup>) of all 21 surface sediment TEX<sub>86</sub><sup>L</sup> values (Rodrigo-Gámiz et al., 2015; this study)

against seasonal and annual temperature depth integrations. B) Calibration of Icelandic marine surface sediment  $\text{TEX}_{86}^{\text{L}}$  values against winter 0-200 m temperature, where gray lines denote the 95% confidence envelope. Surface sediment data shown as closed circles ([this study](#)) and open circles ([Rodrigo-Gámiz et al., 2015](#)).

**Fig. 5:** Comparison of the available  $\text{TEX}_{86}^{\text{L}}$  temperature calibrations on the B997-316 GGC sediment record. Icelandic winter subsurface temperature ([this study](#)), annual SST ([Kim et al., 2010](#)) and annual subsurface temperature ([Kim et al., 2012](#)). Modern (1995-2004 CE) winter subsurface temperature at the B997-316 GGC site marked with gray dashed line ([Locarnini et al., 2010](#)).

**Fig. 6:** Comparison of select B997-316 GGC marine climate proxies to other well-dated Icelandic NIS marine climate records. A) B997-316 GGC  $\text{IP}_{25}$  concentrations ([this study](#)), B) triene Z concentrations ([this study](#)), C) MD99-2275 alkenone-inferred SST ([Sicre et al., 2011](#)), D) B997-316 GGC GDGT-inferred subsurface temperatures, with values below the record mean (4.34 °C) highlighted in blue ([this study](#)), and E) schlerochronological  $\Delta R$  record, where increases in  $\Delta R_{\text{shell}}$  values reflect the incursion of older, Arctic waters ([Wanamaker et al., 2012](#)). Vertical yellow bars highlight the period of interpreted thick sea ice, and the associated insulation/warming of the subsurface. Dashed blue lines bound the inferred periods of LIA-like conditions for the surface (A-C) and subsurface (D).



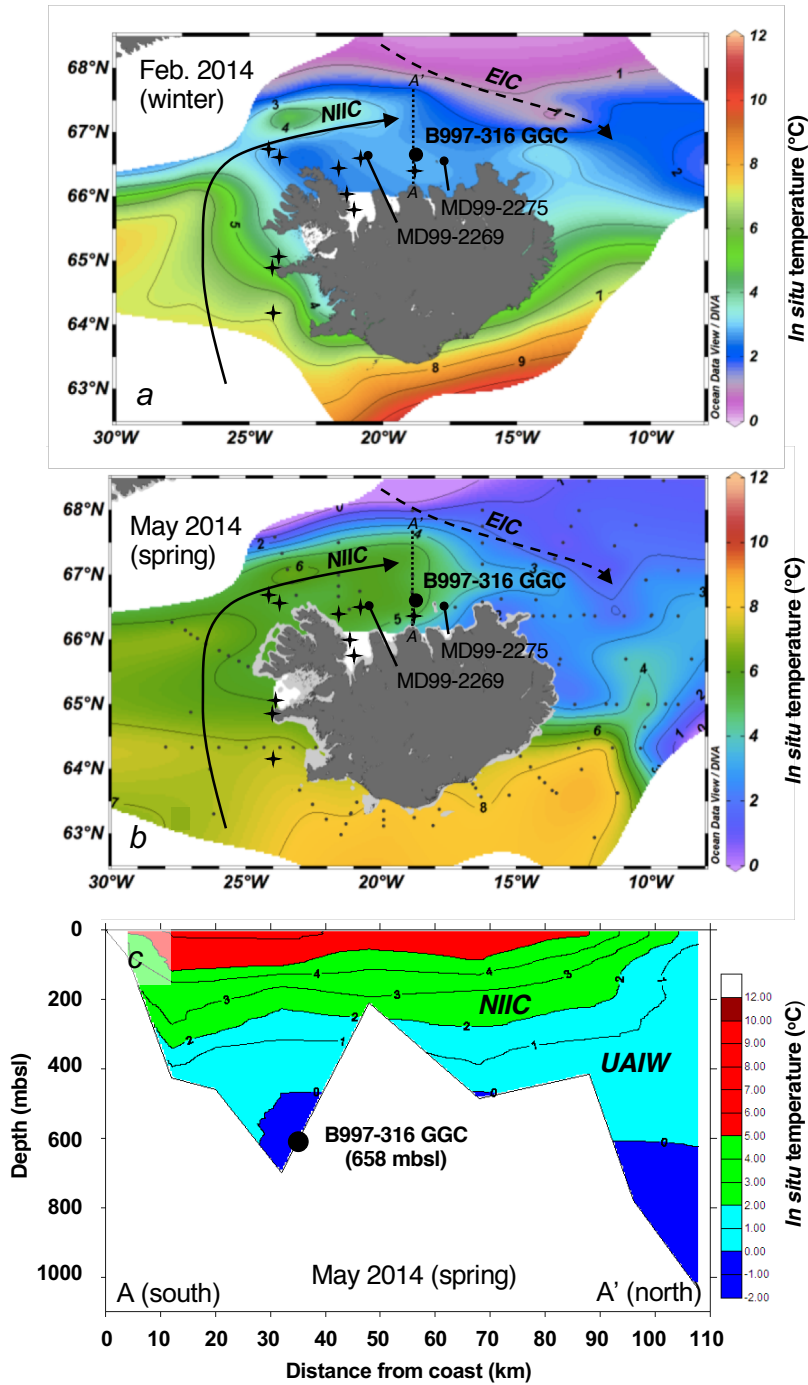


**Fig. 1:** A) Overview maps of modern Icelandic oceanography. A) February 2014 and B) May 2014 50 m depth potential temperature integrated from local CTD stations. Marine sediment cores (black dots) and used B997 surface sediment sample locations (black + and B997-316 GGC core site) are marked. C) May 2014 S-N trending cross section of NIS bathymetry and vertical potential temperature structure along the Siglunes transect and through the B997-316 GGC marine sediment core site. Data from Hafrannsóknastofnun ([Marine and Freshwater Research Institute, http://www.hafro.is/Sjora/](http://www.hafro.is/Sjora/)).

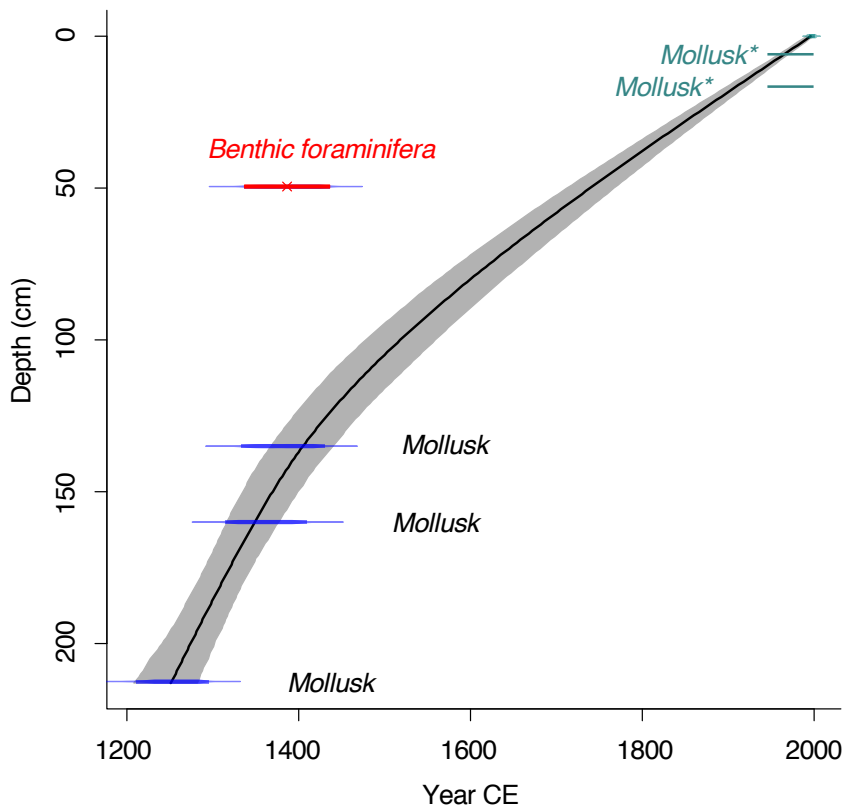


**Fig 2:** CLAM age model. Gray shaded area denotes the 95% confidence envelope (Blaauw, 2010). Teal and asterisked mollusk ages are from the adjacent short gravity core, B997-316 SGC, and not used as age control points in this model. Radiocarbon information provided in Table 1.

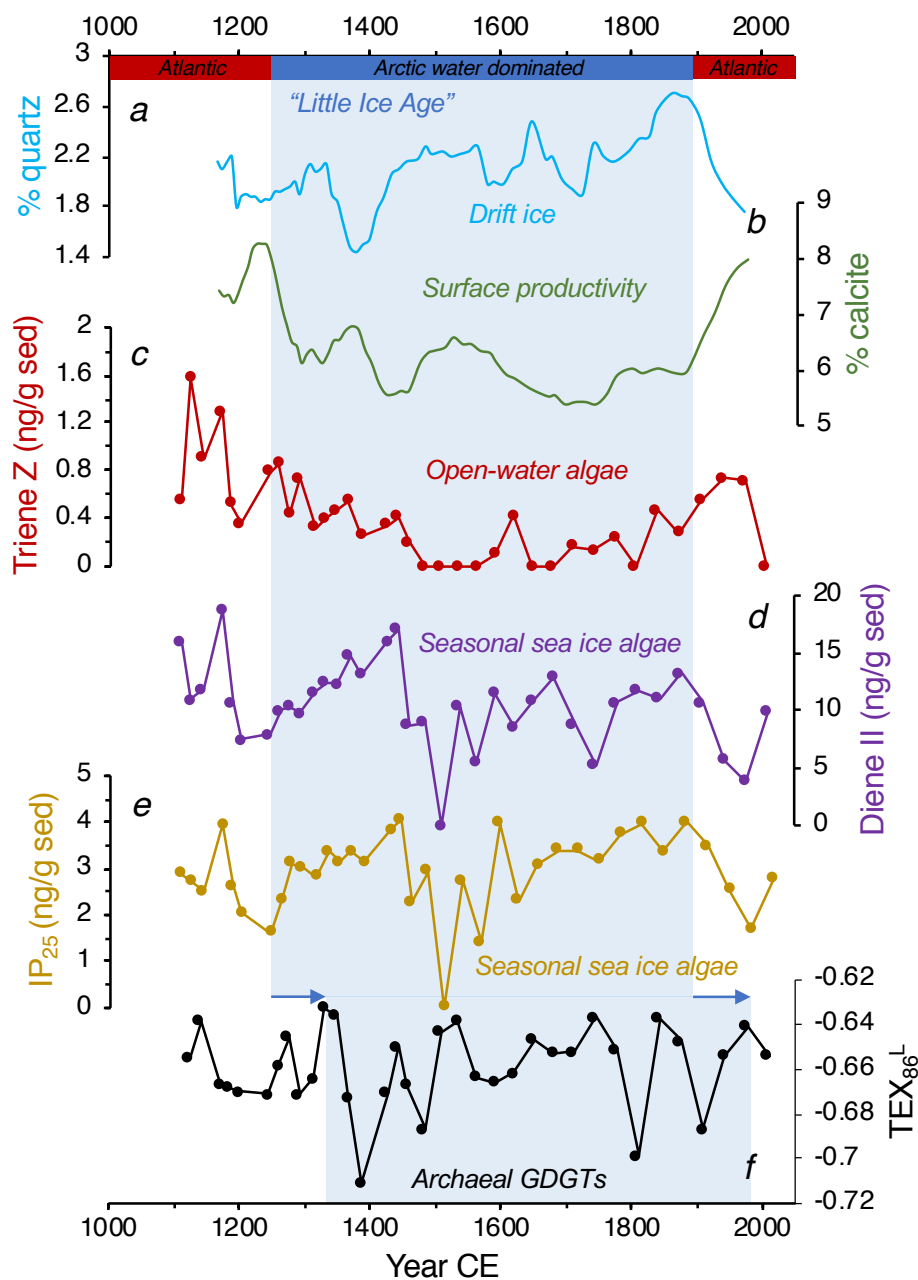


**Fig. 3:** B997-316 GGC marine sediment core climate proxies over the last millennium. A) % quartz, B) % calcite, C) triene Z concentrations, D) diene II concentrations, E) IP<sub>25</sub> concentrations, and F) TEX<sub>86</sub><sup>L</sup>. Blue boxes highlight colder, LIA-like conditions reflected in the surface climate proxies (A-E) and the subsurface proxy (F).

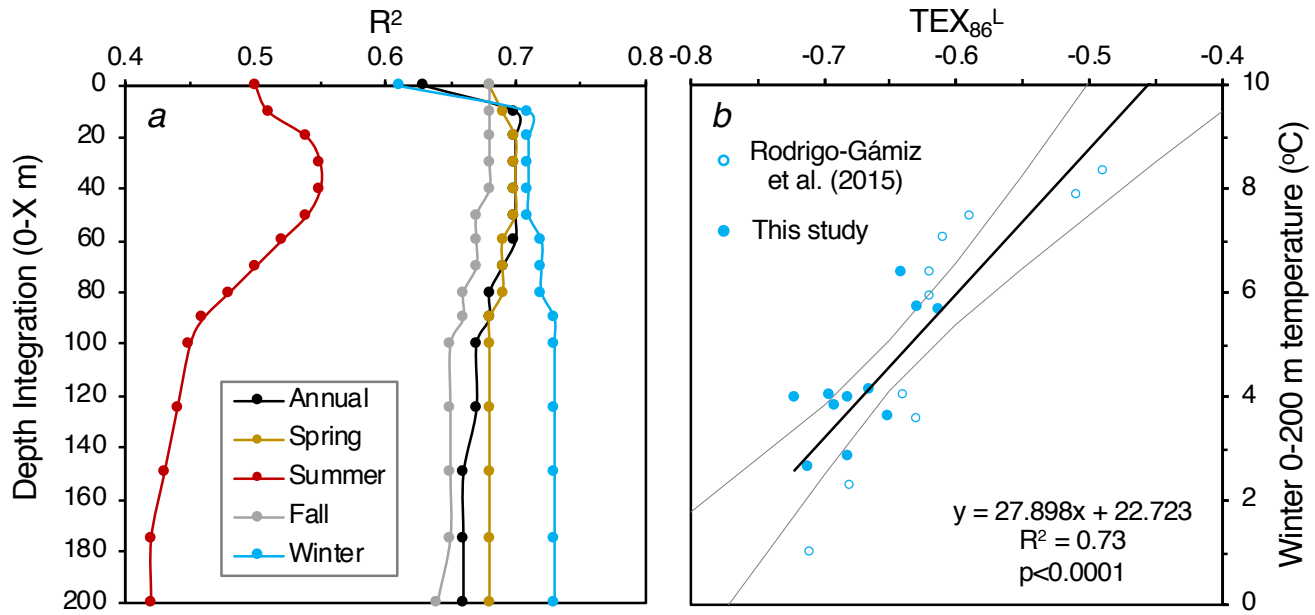


**Fig. 4:** Regression analysis summary of surface sediment GDGT calibration. A) Correlation coefficient ( $R^2$ ) of all 21 surface sediment  $\text{TEX}_{86}^L$  values against seasonal and annual temperature depth integrations. B) Calibration of Icelandic marine surface sediment  $\text{TEX}_{86}^L$  values against winter 0-200 m temperature, where gray lines denote the 95% confidence envelope. Surface sediment data shown as closed circles ([this study](#)) and open circles ([Rodrigo-Gámiz et al., 2015](#)).

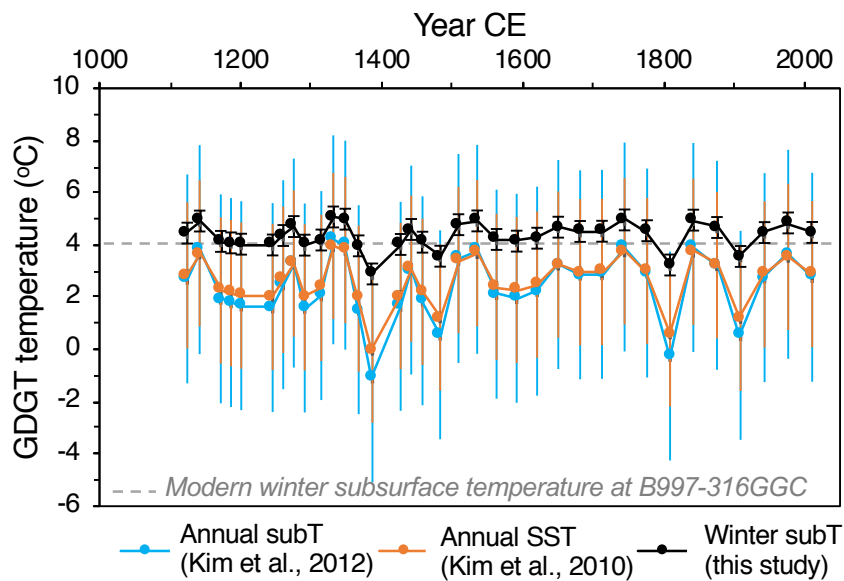


**Fig. 5:** Comparison of the available  $\text{TEX}_{86}^L$  temperature calibrations on the B997-316 GGC sediment record. Icelandic winter subsurface temperature ([this study](#)), annual SST ([Kim et al., 2010](#)) and annual subsurface temperature ([Kim et al., 2012](#)). Modern winter subsurface temperature at the B997-316 GGC site marked with gray dashed line.

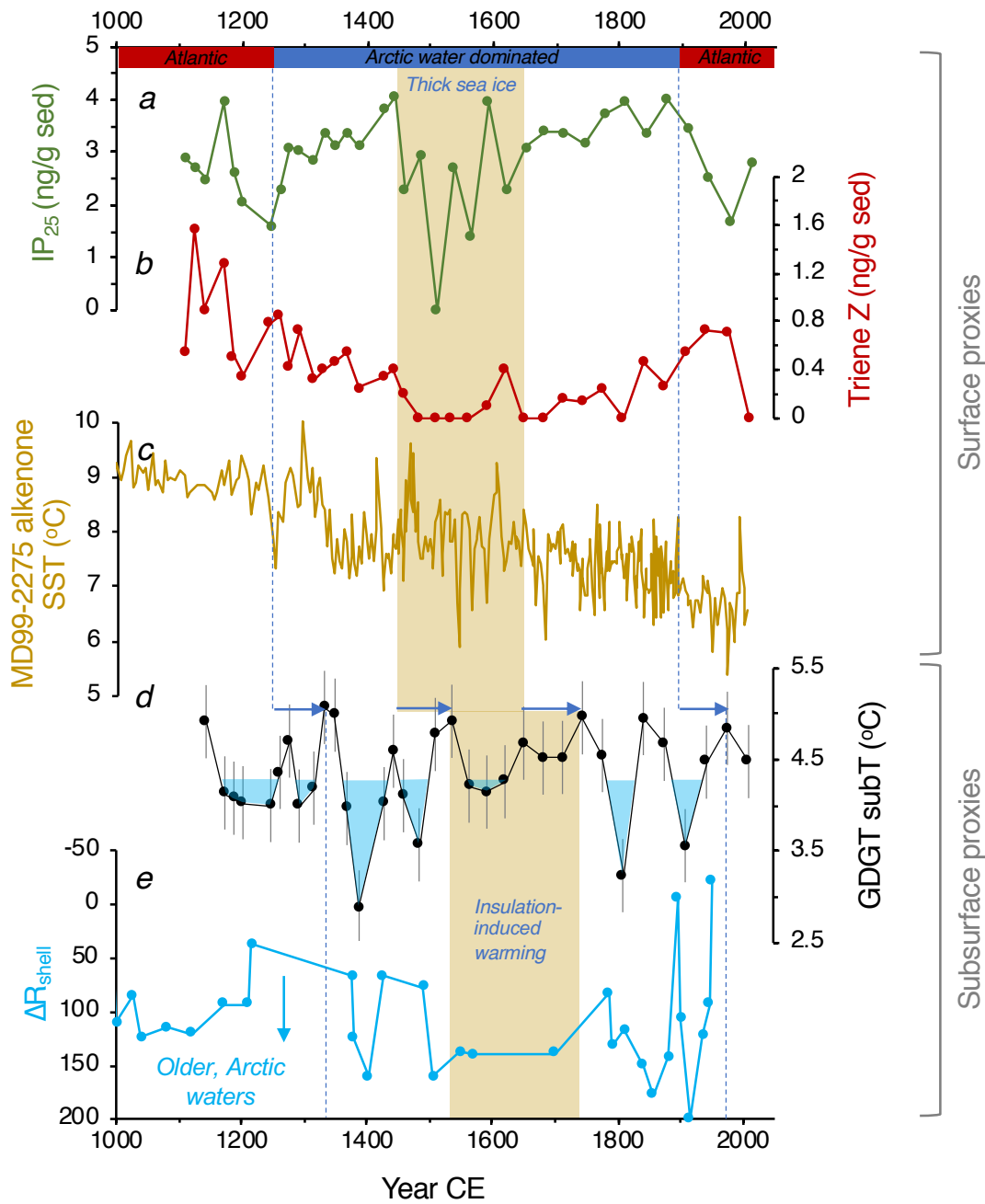
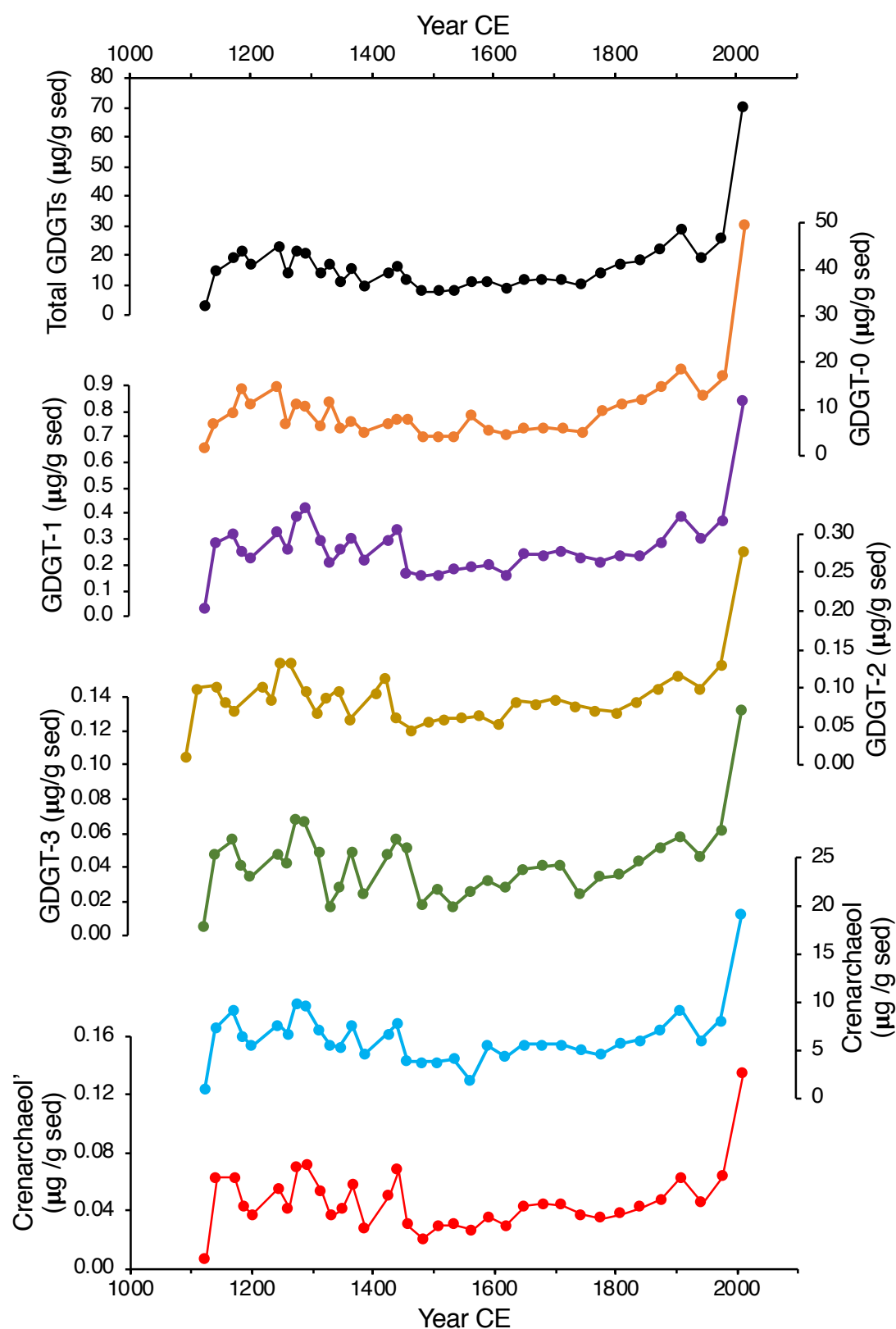
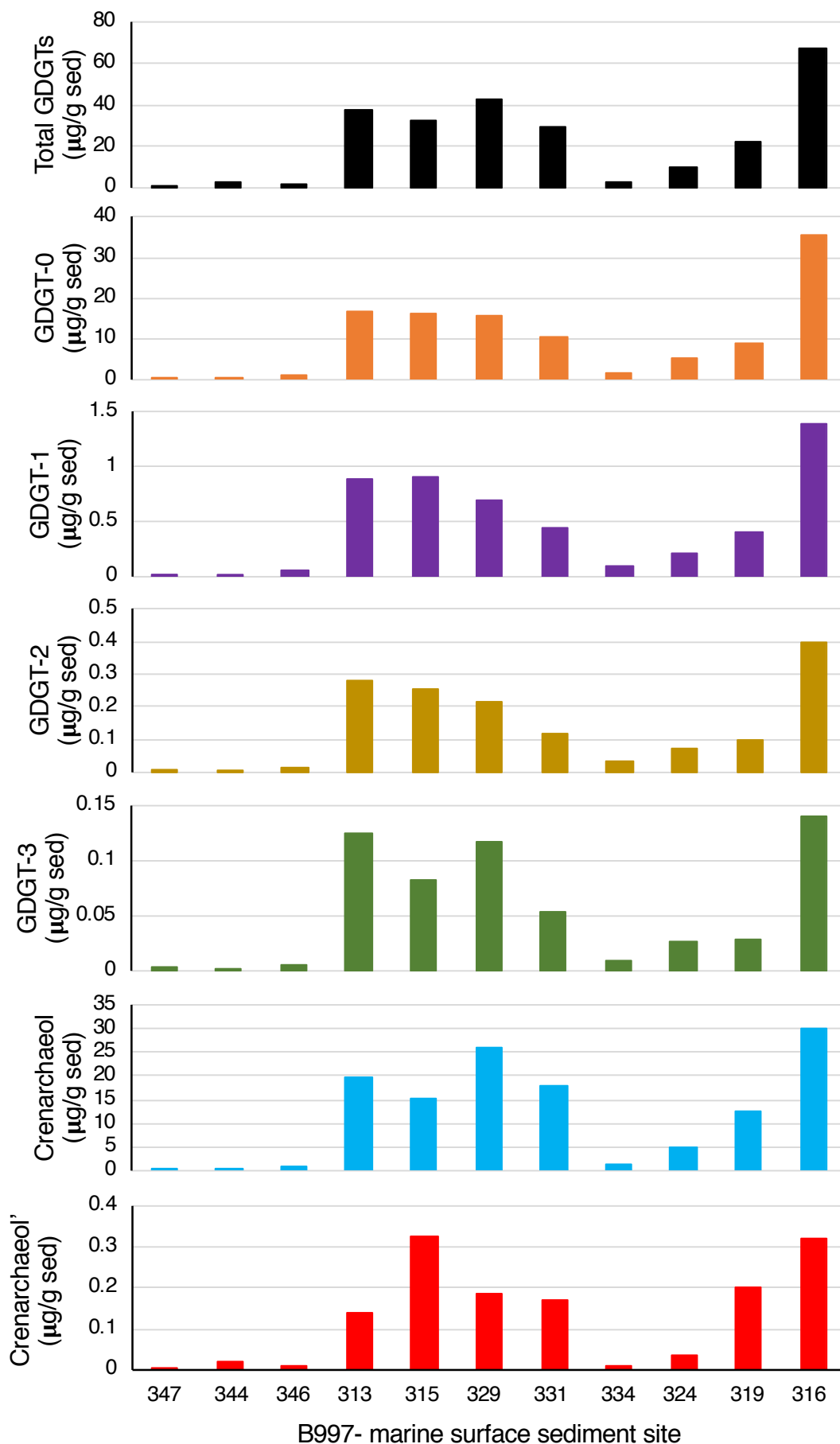


**Fig. 6:** Comparison of select B997-316 GGC marine climate proxies to other well-dated, high-resolution Icelandic NIS marine climate records. A) B997-316 GGC  $IP_{25}$  concentrations ([this study](#)), B) Triene Z concentrations ([this study](#)), C) MD99-2275 alkenone-inferred SST ([Sicre et al., 2011](#)), D) B997-316 GGC GDGT-inferred subsurface temperatures, with values below the record mean highlighted in blue ([this study](#)), and E) schlerochronological  $\Delta R$  record, where increases in  $\Delta R_{shell}$  values reflect the incursion of older, Arctic waters, and a weaker AMOC ([Wanamaker et al., 2012](#)). Vertical yellow bars highlight the period of interpreted thick sea ice, and then the delayed associated insulation/warming of the subsurface. Dashed blue lines bound the inferred periods of LIA-like conditions for the surface (A-C) and subsurface (D) proxies.

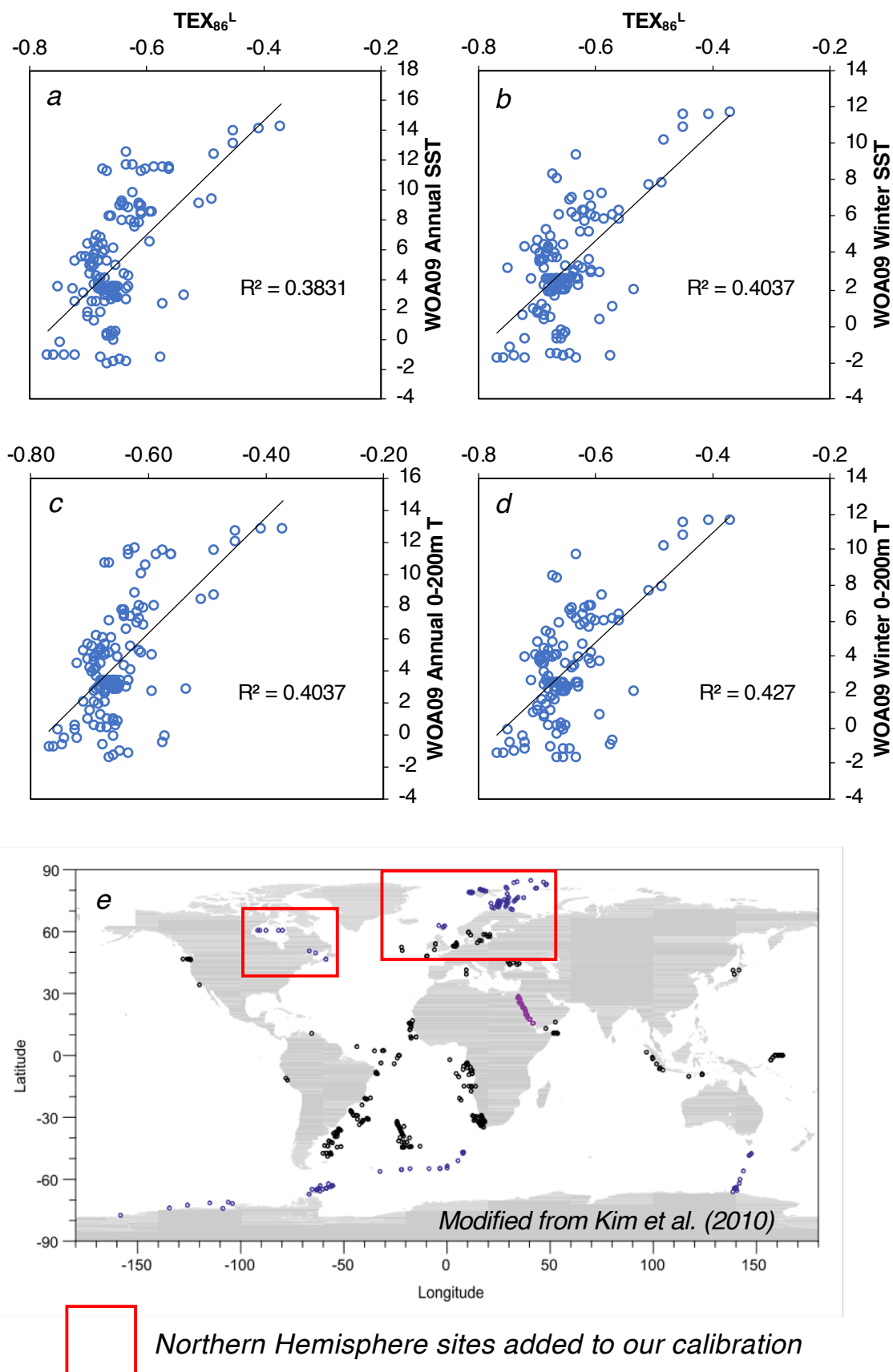


**Supplemental Fig S1:** GDGT concentrations in B997-316 GGC marine sediment samples.



**Supplemental Fig S2:** GDGT concentrations in B997 marine surface sediment samples. Sample labels are abbreviated (i.e., 347 = B997-347) and ordered geographically from the southwestern-most (347, left) to the northeastern-most (316, right).





**Supplemental Fig S3:** Using samples selected from the global calibration of Kim et al. (2010) we tested whether we could improve the local calibration by extending the range of samples, and thus, the environmental gradient. A) Annual SST, B) Winter SST, C) Annual 0-200 m T, and D) 0-200m T. Panel E highlights the northern hemisphere samples included from the the global calibration of Kim et al. (2010).